Transmission of blue (S) cone signals through the primate lateral geniculate nucleus

C. Tailby[1,2,3], B. A. Szmajda[1,2], P. Buzás[1,2], B. B. Lee[4,5] and P. R. Martin[1,2]

[1]*National Vision Research Institute of Australia, Melbourne, Australia*

[2]*Department of Optometry and Vision Sciences, University of Melbourne, Australia*

[3]*Discipline of Physiology, School of Medical Sciences and Bosch Institute, University of Sydney, Australia*

[4]*State University of New York, State College of Optometry, New York, USA*

[5]*Max Planck Institute for Biophysical Chemistry, Göttingen, Germany*

This study concerns the transmission of short-wavelength-sensitive (S) cone signals through the primate dorsal lateral geniculate nucleus. The principal cell classes, magnocellular (MC) and parvocellular (PC), are traditionally segregated into on- and off-subtypes on the basis of the sign of their response to luminance variation. Cells dominated by input from S-cones ('blue-on and blue-off') are less frequently encountered and their properties are less well understood. Here we characterize the spatial and chromatic properties of a large sample of blue-on and blue-off neurons and contrast them with those of PC and MC neurons. The results confirm that blue-on and blue-off cells have larger receptive fields than PC and MC neurons at equivalent eccentricities. Relative to blue-on cells, blue-off cells are less sensitive to S-cone contrast, have larger receptive fields, and show more low-pass spatial frequency tuning. Thus, blue-on and blue-off neurons lack the functional symmetry characteristic of on- and off-subtypes in the MC and PC pathways. The majority of MC and PC cells received no detectable input from S-cones. Where present, input from S-cones tended to provide weak inhibition to PC cells. All cell types showed evidence of a suppressive extra-classical receptive field driven largely or exclusively by ML-cones. These data indicate that S-cone signals are isolated to supply the classical receptive field mechanisms of blue-on and blue-off cells in the LGN, and that the low spatial precision of S-cone vision has origins in both classical and extraclassical receptive field properties of subcortical pathways.

The first stage of human colour vision is the activation of cone photoreceptors that are maximally sensitive to short (S), medium (M) or long (L) wavelengths of the visible spectrum (Young, 1802; Gegenfurtner & Kiper, 2003). The S-cones constitute only a small fraction (5–10%) of cone photoreceptors in diurnal primates, and the nature and distribution of S-cone signals in subcortical pathways remain poorly understood. Studies of macaque species (Mariani, 1984; Kouyama & Marshak, 1992; Dacey *et al.* 1996; Lee & Grünert, 2007) and of two species of New World monkey (marmoset, *Callithrix jacchus*, and capuchin monkey, *Cebus apella*; Silveira *et al.* 1999; Lee *et al.* 2005; Lee & Grünert, 2007) show that S-cone pathways are anatomically segregated at the earliest stages of retinal processing, and that the signals arising in S-cones provide little functional input to midget-parvocellular (PC) and parasol-magnocellular (MC) ganglion cells (Sun

et al. 2006*a*,*b*). The question whether the functional isolation exhibited in the retinal efferent stream is preserved in the dorsal lateral geniculate nucleus (LGN) remains, however, controversial: for example, reports of S-cone inputs to MC relay cells in macaque monkeys vary from negligible input to ∼10% (Derrington *et al.* 1984; Chatterjee & Callaway, 2002; Reid & Shapley, 2002; Solomon & Lennie, 2005). As the majority of synapses in the LGN are of extra-retinal origin (for review, see Sherman & Guillery, 2006) there is obvious potential for feed-forward and/or feed-back 'crosstalk' of S-cone signals among relay cell populations. Understanding the functional segregation of S-cone signals is important for understanding colour vision and has clinical relevance, because increases in S-cone detection thresholds have been used as an early sign of blinding diseases such as glaucoma (Felius & Swanson, 2003; Ferreras *et al.* 2007).

The low density of cells with S-cone input, in both retina and LGN, has hampered their study by *in vivo* recording techniques. In Old World (macaque) and New World (marmoset) monkeys there exist two specialized ('blue-on' and 'blue-off') receptive field classes which are dominated by functional input from S-cones (Dacey & Lee, 1994; Kremers *et al.* 1997; Chichilnisky & Baylor, 1999; Dacey & Packer, 2003; Dacey *et al.* 2005; Field *et al.* 2007), but low encounter rates in both retina and LGN have made it difficult to gather adequate cell samples (Malpeli & Schiller, 1978; DeMonasterio, 1979; Zrenner & Gouras, 1981; Zrenner & Gouras, 1983; Derrington *et al.* 1984; Valberg *et al.* 1986; Reid & Shapley, 2002; Dacey & Packer, 2003; Szmajda *et al.* 2006; Field *et al.* 2007). It is now known that in marmosets the koniocellular layer K3 (between the PC and MC layers) contain a comparatively high density of cells with S-cone input (Martin *et al.* 1997; Szmajda *et al.* 2006). In marmosets, layer K3 is relatively large and can be easily targeted. In previous studies we exploited this anatomical segregation to study the spatial properties of blue-on and blue-off cells (Szmajda *et al.* 2006) and to compare the functional weight of S-cone inputs to MC and PC cells at low and optimal spatial frequency (Hashemi-Nezhad *et al.* 2008). In the present study we re-analysed and added to the dataset described by Szmajda *et al.* (2006). Our goal is to extend our previous studies by establishing how S-cone signals contribute to linear (classical) and nonlinear (extraclassical) receptive field mechanisms. Although different aspects of this question have been addressed in previous studies, a comprehensive comparison of the major classes of geniculate neuron (PC, MC, blue-on and blue-off) under uniform stimulus conditions has not been made. Here we use a modification of a recently developed, robust, method for estimating the functional weight of cone inputs to the classical receptive field (Sun *et al.* 2006*a*,*b*). We combined this method with spatial frequency and aperture tuning measurements to estimate the contribution of S-cones to extraclassical receptive field mechanisms. By drawing together data from large numbers of cells we also hope to determine whether variation in receptive field properties is due to the presence of discrete subpopulations among the main cell classes.

Methods

Extracellular recordings of neurons in the LGN were taken from 29 adult marmosets (*Callithrix jacchus*) of body weight 280–470 g. Animals were obtained from the Australian National Health and Medical Research Council (NHMRC) combined breeding facility. Fourteen of the animals were female. Procedures were approved by the Institutional Animal Ethics Committee, and conformed to the Society for Neuroscience and Australian National Health and Medical Research Council policies on the use of animals in neuroscience research. The ML-cone complement for the majority of animals ($n = 21$) was predicted prior to the extracellular recording experiments, by polymerase chain reaction-run length fragment polymorphism analysis of the ML-cone opsin-encoding genes as previously described (Blessing *et al.* 2004).

Animals were anaesthetized with inhaled isoflurane (Forthane, Abbott, Sydney, 1.5–2%) and intramuscular ketamine (Ketalar, Parke-Davis, Sydney, 30 mg kg^{-1}) for surgery. A femoral or tail vein and the trachea were cannulated. Animals were artificially respired with a 70%–30% mixture of NO_2–Carbogen (5% CO_2 in O_2). A venous infusion of 40 mg kg^{-1} alcuronium chloride (Alloferin, Roche, Sydney) in dextrose Ringer solution was infused at a rate of 1 ml h^{-1} to maintain muscular relaxation. Anaesthesia was maintained during recording with a venous infusion of sufentanil citrate (Sufenta-Forte, Janssen-Cilag, Beerse, Belgium; 4–12 μg kg^{-1} h^{-1}). Electroencephalogram (EEG) and electrocardiogram signals were monitored. Dominance of low frequencies (1–5 Hz) in the EEG recording, and stability of the EEG frequency spectrum under intermittent noxious stimulus (tail-pinch) were taken as the chief signs of an adequate level of anaesthesia. We found that low anaesthetic dose rates in the range cited above were always very effective during the first 24 h of recording; thereafter if drifts towards higher frequencies in the EEG record became evident, they were counteracted by increasing the rate of venous infusion. The typical duration of a recording session was 48–72 h. At the termination of the recording session the animal was killed by intra-venous delivery of an overdose of pentobarbitone sodium (80–150 mg kg^{-1}).

Visual stimulation and data aquisition

Data consisted of responses of LGN neurons to drifting sinusoidal gratings and sinusoidal temporal modulation of spatially uniform fields. Action potentials arising from visually responsive cells were identified and the time of their occurrence measured to an accuracy of 0.1 ms. Responses were subjected to Fourier analysis; the first harmonic amplitude and phase were used as response measures.

Each visually responsive cell was initially classified using hand-held stimuli and its receptive field mapped on the tangent screen. In early experiments visual stimuli were generated using a Series Three video signal generator (VSG Series Three, Cambridge Research Systems, Cambridge, UK) and presented on a Reference Calibrator Plus monitor (Barco) at a frame refresh rate of 80 Hz. The VSG system incorporates a photometric feedback system for colourimetric specification and gamma correction to allow direct specification of stimuli in CIE (x, y, Y) coordinates. In later experiments visual stimuli were

generated using Open GL commands controlled via freely available software (Expo, Peter Lennie) and presented on a linearized, colourimetrically calibrated Sony G520 monitor refreshed at 120 Hz. The accuracy of both systems was verified with a PR-650 photometer (Photo Research, Palo Alto, CA, USA).

For each cell, the optimal spatial frequency, temporal frequency, orientation and contrast was determined, using achromatic drifting gratings presented within a 4 deg diameter aperture at a mean luminance of 55 (Expo) or 32 (VSG) cd m^{-2}. An aperture-tuning curve was measured using the optimum stimulus parameters. An aperture diameter which was slightly above the optimal diameter, and which also was an integer multiple of the optimum spatial period, was used thereafter. The reader should note that such apertures encompass both centre and surround components of the classical receptive field (Solomon *et al.* 2002). Receptive field dimensions were estimated by difference-of-Gaussians (DOG) fitted to the spatial-frequency tuning curve using standard methods (Croner & Kaplan, 1995; White *et al.* 2001). At the low temporal frequencies used for these measurements (4–5 Hz), the phase error introduced by using the DOG fit rather than a vector model (Frishman *et al.* 1987; Kilavik *et al.* 2003) is small (< 15 deg).

Characterization of cone inputs

A set of spectral absorbance templates (nomograms) with peak wavelengths corresponding to those present in a given animal was generated using the polynomial templates of Baylor *et al.* (1987) or Lamb (1995). Lens absorbance was corrected using published measurements for marmoset (Tovée *et al.* 1992). The effect of receptor self-screening was estimated assuming axial absorbance of 1.5% and outer segment length 20 μm. For measurements taken using the VSG system, the cone contrast for a given stimulus was calculated for each nomogram by convolution with the (x, y, Y) coordinates of the grating components *via* the Judd–Voss modified CIE 1931 colour matching functions (Brainard, 1996). For measurements taken using the Expo system, the contrast in a given class of cone generated by a given stimulus was obtained by calculating the inner product between the relevant cone nomogram and the spectral power distribution of the R, G, and B guns specified by the stimulus. The resulting inner products (corresponding to cone activations elicited separately by the R, G, and B guns) were then summed and expressed relative to their values at the white point (R, G, and B guns set to the mean value), calculated in the same manner.

Estimating the strength of S-cone inputs

We estimated the strength of S-cone inputs to the receptive fields of LGN cells using two methods. Both methods use modulations in chromaticity and luminance

to extract the functional weight of S-cone inputs by the amplitude and/or phase of cell response. The first method, hereinafter described as the 'colour circle' method, is described in detail by Sun *et al.* (2006*a*). The second, hereinafter described as the 'colour vector' method, is described in detail by Hashemi-Nezhad *et al.* (2008). The two methods have distinct advantages: the colour circle method allows rapid assessment of cone weights given *a priori* knowledge of the ML-cone-opsin encoding genes, whereas the colour vector method is slower but does not depend on calculation of cone-selective stimuli. We show below that the two methods give similar results.

In the colour circle method (Sun *et al.* 2006*a*) the chromaticity of a uniform field is modulated around the circumference of a colour circle. The colour circle lies on a plane defined by an S-cone modulation axis and an ML-cone modulation axis. An angle of 0 deg in this plane corresponds to an increase in the activation of ML-cones with no change in the activation of S-cones; 90 deg corresponds to increased activation of S-cones with no change in the activation of ML-cones. The maximu ML and S-cone contrasts attained during modulation around the circle were set to 50%. For a cell that receives cone inputs weight w_S from S cones, and w_{ML} from ML cones, the preferred response vector (θ_{pref}) is determined by the amplitude and phase of the combined cone inputs. The preferred vector was estimated by averaging the cell's response phase for clockwise and counter-clockwise modulations around the colour circle. This averaging procedure serves to discount the phase lag due to response latency. We measured responses to five temporal frequencies (± 1, ± 2, ± 4, ± 8, ± 16 Hz). We define clockwise modulations as negative temporal frequencies, counter-clockwise modulations as positive. The relative weight of S and ML-cone input was recovered as described in Sun *et al.* (2006*a*).

In the colour vector method, responses to chromatic-spatial variation were measured using sinusoidal gratings that were modulated in 144 or 62 directions about a white point (CIE D65) at a mean luminance of 32 cd m^{-2}. The maximum achromatic Michelson contrast was 48%. Grating vectors were uniformly spaced excursions in chromaticity (CIE x, y) and luminance (CIE Y). Predicted responses of receptors with peak sensitivity at 423 nm (S-cone), 543, 556, or 563 nm (ML-cones) were fitted to the form:

$$R = A[wC_1 + (1 - |w|)C_2],$$

where R is the predicted response amplitude, A is an amplitude scaling factor, C_1 and C_2 are receptor contrasts, and w is a weighting factor which can vary between -1 and $+1$. Negative values of w represent out-of-phase (opponent) combination; positive values represent in-phase (additive) combinations. To make the

results of this method compatible with the results of the colour circle method, the signs of S- and ML-cone inputs were recovered by reference to the response sign for achromatic modulation (for PC and MC cells) or for S-cone modulation (for blue-on and blue-off cells). For trichromatic animals the single receptor response C_2 was replaced by a variable-weighted sum of M and L response. Responses were fitted in the complex plane using Euler's equation $R = a e^{i\phi}$, where R is the complex-valued response vector, a is response amplitude, e is the natural exponent, i is $\sqrt{-1}$, and ϕ is response phase. The latency between centre and surround mechanisms (~ 5 ms) represents a phase delay of less than 15 deg at the stimulus frequency we used (4–5 Hz), and was omitted from the calculations. Data were fitted to the model by constrained nonlinear optimization of F1 amplitude and phase (*fmincon*, Matlab optimization toolbox, v. 2, The MathWorks Inc., Natick, MA, USA).

Location of recorded cells

The position of each recorded cell was noted by reading the depth from the hydraulic microelectrode advance (David Kopf Model 640). Assignment to parvocellular and magnocellular categories was, in the great majority of cases, straightforward. Cells in these classes show stereotyped response properties. Furthermore, transitions across parvocellular and magnocellular laminae are marked by eye dominance changes, and by characteristic changes in background multiunit activity. We therefore use the terms parvocellular (PC) cells and magnocellular (MC) cells in the present paper to refer to receptive fields with the characteristics of these respective populations.

We previously showed that the majority of blue-on and blue-off receptive fields is segregated to the koniocellular (KC) layers (Martin *et al.* 1997; White *et al.* 1998; Szmajda *et al.* 2006; Hashemi-Nezhad *et al.* 2008). In the present study we retain the terms blue-on and blue-off rather than referring to these populations as KC cells. The purpose of this nice distinction is to emphasize the heterogeneous nature of the KC pathway, for example many KC cells in marmosets do not receive S-cone inputs (Solomon *et al.* 1999; White *et al.* 2001; Solomon *et al.* 2002). Receptive fields with 'non-standard' properties were encountered in the present study (Irvin *et al.* 1986; Solomon *et al.* 1999; White *et al.* 2001), but their chromatic inputs were not systematically measured. In some animals in the present study (14/39), electrolytic lesions (6–10 μA $\times$ 6–10 s, electrode negative) were made to mark selected recording positions, and the position of recorded cells in the LGN was subsequently reconstructed. As described (Szmajda *et al.* 2006), no clear differences in the properties of blue-on and blue-off cells recorded in different LGN layers were apparent so the data were pooled.

Results

We show here data collected from 513 neurons encountered in LGN of 29 marmosets (16 male). Seventeen of these animals were dichromatic, expressing S-cones (peak $\sim$423 nm) and a second cone class in the medium–long (ML) wavelength sensitive range peaking near 543 nm ($n = 9$), 556 nm ($n = 6$), or 563 nm ($n = 2$). Of the trichromatic animals three expressed M- and L-cones at peaks of 543 nm and 556 nm, seven expressed peaks at 543 nm and 563 nm, and two expressed peaks at 556 nm and 563 nm. The dataset included cells analysed in our previous study of the segregation of blue-on and blue-off cells to the koniocellular layers in marmosets (Szmajda *et al.* 2006; PC cells, 89/349 (25%); MC cells, 0/89 (0%); blue-on cells, 36/59 (61%); blue-off cells, 14/16 (88%)). Not all tests were carried out on all cells. Where applicable, spatial tuning data for achromatic stimuli reported in a previous study (Forte *et al.* 2005) were reanalysed for the present study.

The absorption spectra of the different subtypes of marmoset cone are not known as precisely as those of the human, and the profile of macular pigment density in this species is also uncertain. We did not correct for macular pigment as the majority of receptive fields (472/513, 92%) were located more than 1 deg from the foveola. We refer to stimulus conditions as S-cone selective and ML-cone selective, but it is of course possible that variations in prereceptoral absorption make these stimuli deviate slightly from the optimal cone selective lines. The potential influence of 'bleed-through' of signals from nominally silent cones is especially problematic for high gain cells such as MC cells. We have handled this ineluctable difficulty in a variety of ways, discussed at appropriate points in the text.

Identification of blue-on and blue-off cells

Figure 1 shows spatial frequency tuning (left column) and contrast response functions (centre column), measured with achromatic (open symbols) and S-cone selective gratings (filled symbols), for four example LGN neurons encountered at comparable eccentricities. The blue-on and blue-off cell respond strongly to both achromatic and S-cone selective modulations, being at least as sensitive to S-cone modulation as to achromatic modulation (Fig. 1*B* and *D*). The PSTHs in the right-hand column of the figure show further that these cells respond to opposite phases of a low spatial frequency S-cone selective stimulus (0.01 cycle deg^{-1}, temporal frequency 5 Hz): the discharge of the cell in Fig. 1*A* increases during the increment phase; that of the cell in Fig. 1*C* during the decrement phase. We refer to these cells as blue-on and blue-off cells, respectively. Response phase reliably differentiated those cells that responded to S-cone modulation into two

non-overlapping groups (separated by ∼160 deg of phase: Szmajda *et al.* 2006). We therefore used response phase to classify those cells that were more responsive to S-cone modulation than achromatic modulation, and discharged at more than 10 imp s^{-1} to our highest contrast S-cone stimulus, as blue-on or blue-off.

The lower two rows of Fig. 1 show measurements from a PC cell and an MC cell. Both cells respond strongly to achromatic stimuli. Their discharge is unaffected by modulation of the S-cones alone, indicating that they receive input exclusively from ML-cones. Below, we describe recordings obtained from 62 blue-on and 16

blue-off cells, and compare their receptive field properties with those of the more familiar PC and MC cells. We first discuss measurements of spatial frequency tuning functions (see *Spatial receptive field structure*), then measurements of contrast response functions (see *Contrast sensitivity*).

Spatial receptive field structure

Early studies indicated that the receptive fields of LGN neurons receiving strong S-cone input lack spatial antagonism (Type II cells; Wiesel & Hubel, 1966;
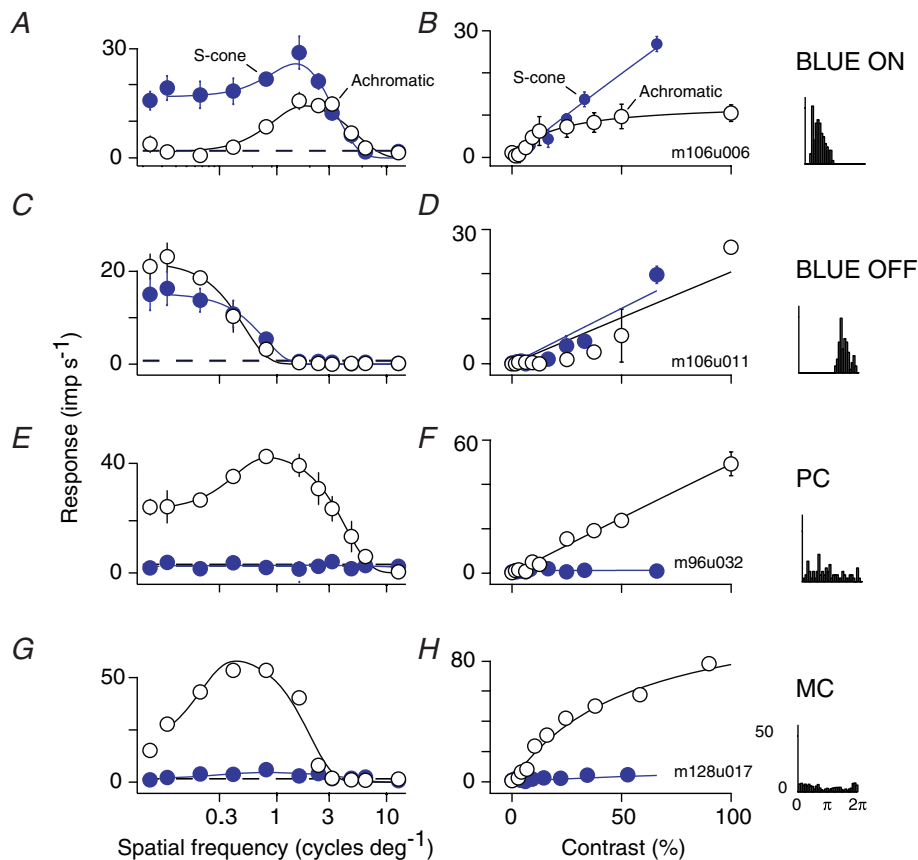

Figure 1. Spatial tuning and contrast sensitivity of different classes of LGN cell
A, spatial frequency tuning of an example blue-on cell for drifting achromatic (open circles) and S-cone selective (filled circles) gratings. Smooth curves show fits of the difference-of-Gaussians model defined in Methods. Error bars show standard errors of the mean (some error bars are smaller than the data symbol). The dashed horizontal line shows the amplitude of the first harmonic in response to a uniform field at the same mean luminance and chromaticity as the gratings. The left-most data point, disconnected from the model fit, shows the response to a drifting grating at a spatial frequency of 0.01 cycle deg^{-1}. *B*, contrast response function for drifting achromatic (open circles) and S-cone selective (filled circles) gratings, recorded from the same cell shown in *A*. Smooth curves show fits of the Naka–Rushton function described in Methods. For both colour directions the spatial frequency was that preferred for S-cone selective stimuli. The rightmost panel shows peri-stimulus time histogram, folded to one cycle of modulation, recorded during presentation of a drifting 0.01 cycle deg^{-1} S-cone selective grating. *C* and *D*, same as *A* and *B* for an example blue-off cell. *E* and *F*, same as *A* and *B* for an example parvocellular cell. In measuring the contrast response function for both colour directions we used the preferred achromatic spatial frequency. *G* and *H*, same as *E* and *F* for an example magnocellular cell.

DeMonasterio & Gouras, 1975; Zrenner & Gouras, 1983). If this is correct their spatial frequency tuning functions should be low-pass. This is the case for the blue-off cell of Fig. 1*C*. It is not the case for the blue-on cell of Fig. 1*A*, however, which shows signs of spatial antagonism for both S-cone selective and achromatic gratings.

The spatial frequency tuning curves of the four example cells shown in Fig. 1 are characteristic of the functional classes to which they belong. Figure 2 shows population average spatial frequency tuning (left column) and contrast response functions (right column) for blue-on, blue-off, PC and MC cells. The average tuning curves shown in each panel include data only from those cells for which both SWS and achromatic tuning curves were obtained. The figure facilitates a direct comparison of the chromaticity-dependent spatial tuning properties of the different cell classes, as each panel contains neurons distributed across a comparable range of eccentricities and measured using the same set of spatial frequencies for each colour direction. This figure has the same format as Fig. 1 but here the error bars show standard deviations in order to indicate variability of response across the populations. In blue-on cells, spatial frequency tuning functions measured with achromatic or S-cone selective gratings are band-pass (Fig. 2*A*; Field *et al.* 2007; Hashemi-Nezhad *et al.* 2008); in blue-off cells they are more low pass (Fig. 2*C*). As expected, the spatial frequency tuning functions of PC cells (Fig. 2*E*) and MC cells (Fig. 2*F*) are bandpass for achromatic gratings and on average there is very little response to S-cone modulations.
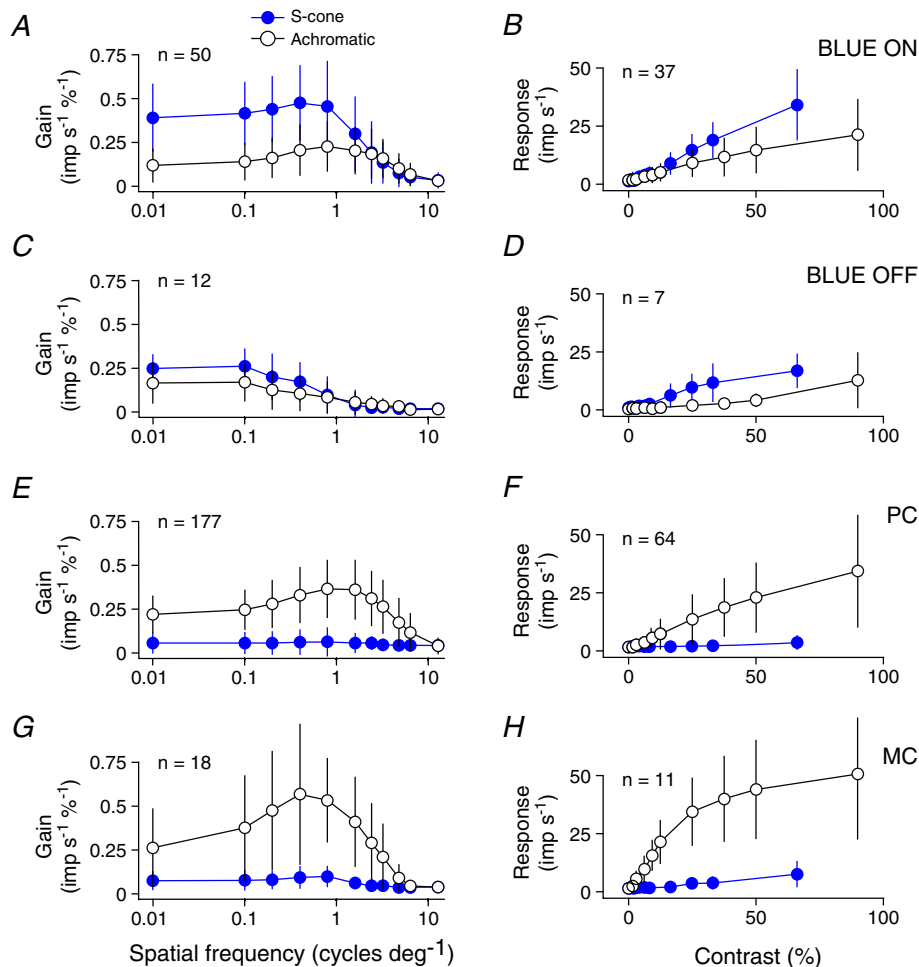

Figure 2. Population average spatial tuning and contrast sensitivity of different classes of LGN cell
Error bars show standard deviations. *A*, average achromatic (open circles) and S-cone selective (filled circles) spatial frequency tuning, calculated across all blue-on cells for which we obtained measurements for both colour directions. *B*, average achromatic (open circles) and S-cone selective (filled circles) contrast response functions calculated across all blue-on cells for which we obtained measurements for both colour directions. *C* and *D*, same as *A* and *B* for blue-off cells. *E* and *F*, same as *A* and *B* for parvocellular cells. *G* and *H*, same as *A* and *B* for magnocellular cells.

Spatial antagonism can be summarized using a single number, which we term the low-cut ratio, calculated as the response to the lowest frequency divided by that to the best frequency. The low-cut ratio can vary between 0 (indicating that responses are completely attenuated at low frequencies) and 1 (indicating that the tuning function is low pass). For all cell classes the low-cut ratio was significantly less than 1 for achromatic gratings ($P < 0.05$, t test). Spatial antagonism was strong in blue-on, PC and MC cells (mean low cut ratios of 0.41 ($n = 61$), 0.57 ($n = 349$), and 0.49 ($n = 47$), respectively) and weaker in blue-off cells (mean low cut ratio $= 0.81$ ($n = 14$)). When measured with S-cone gratings the low cut ratio was also significantly less than 1 ($P < 0.05$) in blue-on cells and blue-off cells (mean $= 0.69$ ($n = 76$) and 0.89 ($n = 16$), respectively). This result implies that the blue-on cells and (to a lesser extent) blue-off cells show weak centre-surround spatial antagonism in S-cone inputs.

The spatial frequency tuning functions shown in Fig. 2 suggest that the receptive fields of blue-on and blue-off neurons are larger than those of PC and MC cells. We evaluated this directly by fitting a difference-of-Gaussians (DOG) model to the tuning curves of individual cells (smooth lines of Fig. 1) and plotting centre radius as a function of eccentricity for the different cell classes. The result is shown in Fig. 3A. We estimated the centre radius (r_c) of PC and MC cells using achromatic gratings ($r_{c\text{-}ACH}$). For blue-on and blue-off neurons we used S-cone selective gratings ($r_{c\text{-}SWS}$).

At any given eccentricity the centre sizes of blue-on and blue-off neurons are larger than those of PC and MC neurons. Figure 3C shows, for cells located within 10 deg of the fovea, the mean centre radii of PC and MC cells measured with achromatic gratings, and of blue-on and blue-off cells measured with S-cone gratings. The receptive fields of blue-off cells are significantly larger than those of all other cell types ($P < 0.05$, ANOVA, Tukey–Kramer *post hoc* test); those of blue-on cells are significantly larger than PC cells ($P < 0.05$) but not MC cells. For both PC and MC cells, on- and off-centre subtypes do not differ significantly in size.

For both blue-on and blue-off cells the centre radius estimated from achromatic gratings tends to be smaller than that for S-cone gratings. We quantified this by calculating the ratio of the centre radii estimated with achromatic and S-cone selective gratings, ($r_{c\text{-}ACH}$)/($r_{c\text{-}SWS}$). This ratio took a geometric mean value of 0.61 for blue-on cells (significantly less than 1, $P < 0.05$, two tailed, paired Wilcoxon's signed rank test), and 0.77 for blue-off cells (Fig. 3B, $P > 0.05$). This suggests that the S and ML mechanisms (both of which are activated by achromatic gratings) do not show exact spatial overlap in these cells.

On the basis of *in vitro* recordings from macaque retina, Dacey *et al.* (2003) reported two populations of blue-on cells with distinct ('small bistratified' and 'large bistratified') dendritic field size. We asked whether the receptive field sizes we measured show signs of bimodal distribution consistent with two blue-on populations. Figure 3E shows, on a linear scale, blue-on and blue-off centre radii for cells recorded within 10 deg of the fovea. There is considerable scatter in the data for blue-on cells (range 0.027–0.77 deg) but the distribution (Fig. 3F) is unimodal ($P = 0.99$, Hartigan dip test). Furthermore the average eccentricity (mean 2.661 deg, S.D. $= 1.984$, $n = 34$) of blue-on cells with centre radius below a criterion of 0.25 deg was lower than that of cells with larger radii (mean 6.199 deg, S.D. $= 1.984$, $n = 10$, $P < 0.01$, Wilcoxon's rank sum test), suggesting that eccentricity-dependent changes underlie much of the variance in the data. The dendritic field diameter of small bistratified cells measured in the central 10 deg of marmoset retina ranged from 0.25 to 0.55 deg (32–70 μm, Szmajda *et al.* 2008); these figures would correspond to centre radii of 0.06–0.13 deg if the dendritic field encompasses 2 Gaussian standard deviations. These values fall close to the peak of the centre size distribution (vertical bar, Fig. 3F), consistent with the idea that inputs to the majority of cells recorded come from small bistratified ganglion cells.

We estimated separately the dimensions of the S and ML-cone receptive fields using cone selective gratings (blue-on: $n = 11$, blue-off: $n = 1$). Recordings from an example blue-on cell are shown in Fig. 4A. We fitted these data with the DOG model and compared the centre radii of S- and ML-cone receptive field components (Fig. 4B). As expected, for blue-on cells the radius of the S mechanism is smaller than that of the ML mechanism estimated from ML stimuli, by an average factor of 0.75 (S.D. $= 0.7$) (Solomon *et al.* 2005; Field *et al.* 2007; Tailby *et al.* 2008). In the one blue-off cell for which we obtained these same measurements, the centre radius estimated from S-cone gratings was ~1.4 times larger than that estimated from ML stimuli.

In summary, these data confirm that at any given eccentricity the receptive fields of most blue-on and blue-off cells are larger than those of PC and MC cells. Blue-on cells and (to a lesser extent) blue-off cells are spatially bandpass – even for gratings that modulate only the S-cones, and the radius of the ML-OFF component of blue-on receptive fields tends to be larger than the S-ON component (Solomon *et al.* 2005; Field *et al.* 2007). The majority of blue-on cells have centre size consistent with input from small bistratified ganglion cells.

Contrast sensitivity

The right column of Fig. 1 shows contrast response functions measured with achromatic and S-cone selective stimuli for the cells shown in the left column of Fig. 1.
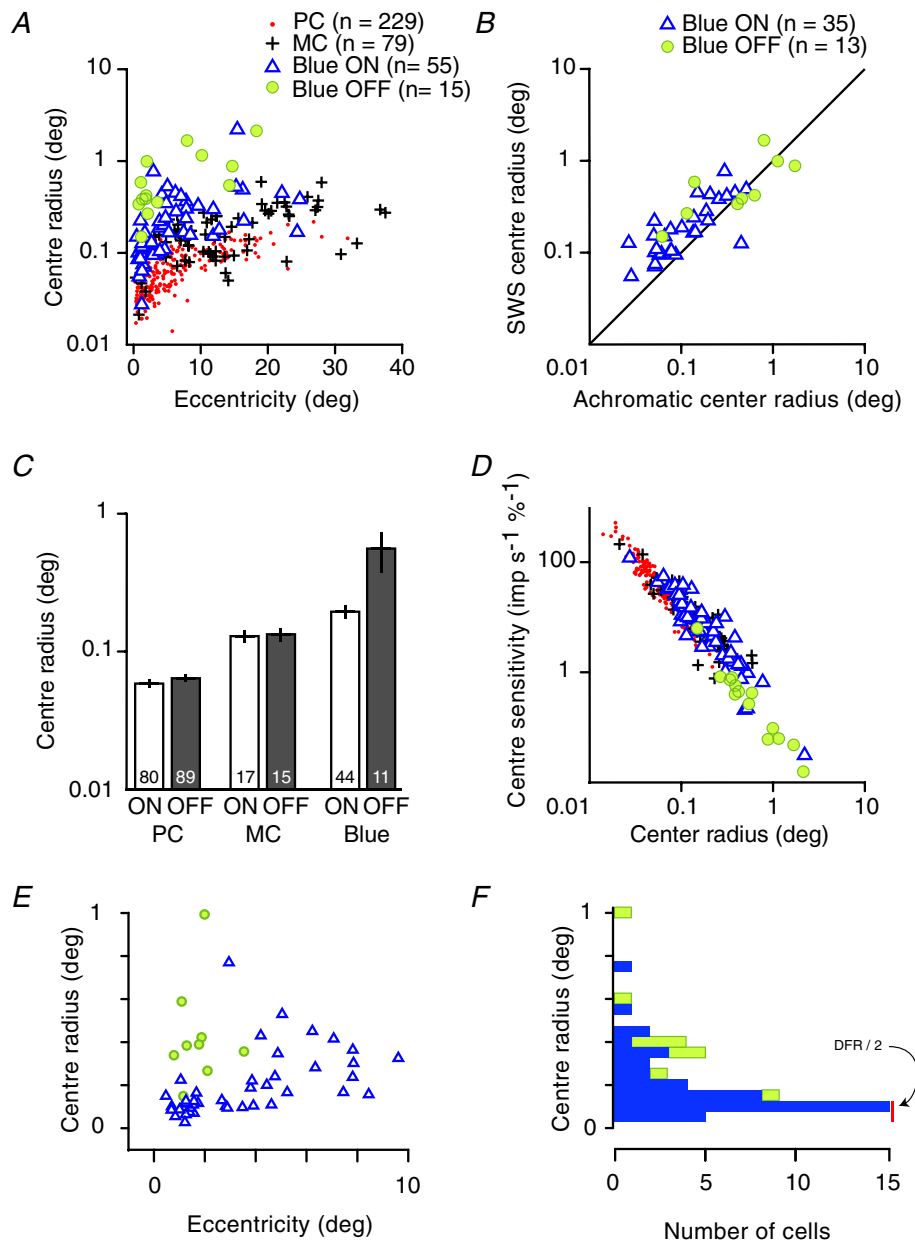
Figure 3. Receptive field centre size and sensitivity

A, centre radius, estimated from difference-of-Gaussian fits, as a function of eccentricity for PC (points), MC (+), blue-on (triangles) and blue-off (filled circles) cells. Centre radius is estimated from achromatic gratings for PC and MC cells, and from S-cone selective gratings for blue-on and blue-off cells. *B*, comparison of the centre radii estimated from achromatic gratings (*x*-axis) and S-cone selective gratings (*y*-axis) in blue-on (triangles) and blue-off (filled circles) cells. *C*, comparison of the mean centre radius of on- and off-centre PC and MC cells, blue-on cells, and blue-off cells. Means are calculated only from cells with receptive fields located within 10 deg of the fovea. Mean radii (and standard errors of the mean) for the different cell types are: PC-on, 0.0586 (0.0033, $n = 80$); PC-off, 0.0639 (0.0032, $n = 89$); MC-on, 0.1291 (0.0138, $n = 17$); MC-off, 0.1328 (0.0149, $n = 15$); blue-on, 0.194 (0.0224, $n = 44$); blue-off, 0.5566 (0. 1821, $n = 11$). *D*, centre sensitivity (k_c) plotted as a function of centre radius (r_c). Conventions as in *A*. *E*, centre radius of blue-on and blue-off cells in the central 10 deg. Blue-off cells have larger centre radius than most blue-on cells at the same eccentricity. *F*, distribution of centre radius within the central 10 deg. Note the unimodal distribution. The vertical bar indicates the anatomical range of dendritic field radius divided by 2 (DFR/2) of small bistratified cells over this eccentricity range (Szmajda *et al.* 2008). This shows that dendritic field radius of small bistratified cells corresponds to approximately ±2 Gaussian standard deviations of the blue-on S-cone mechanism.

For PC and MC cells we measured the contrast response function at the preferred achromatic spatial frequency; for blue-on and blue-off cells we used the preferred spatial frequency for S-cone selective gratings. As expected, the achromatic contrast response of PC cells is essentially linear across the full range of contrasts; that of MC cells rises steeply before beginning to saturate at contrasts above ∼15%. Both blue-on and blue-off cells give reliable responses to achromatic modulation, albeit weaker than that of PC- and MC cells, giving a graded response across the full range of achromatic contrasts.

Blue-on and blue-off cells, as expected, give the strongest responses to S-cone modulation. The S-cone contrast response of both these cell types is approximately linear, with blue-on cells being more responsive. The smooth curves plotted in the right column of Fig. 1 show best fits of the Naka–Rushton function to the contrast response data. These fits were used to estimate the contrast gain of each cell for the two types of stimuli (see Methods). Blue-on and blue-off cells had considerably higher contrast gain for S-cone selective stimuli than they did for achromatic stimuli, with blue-on cells having the highest S-cone gain of any cell class encountered (blue-on: 0.84 imp s^{-1} %$^{-1}$; blue-off: 0.47 imp s^{-1} %$^{-1}$). Most PC and MC cells did not respond reliably to our nominal S-cone isolating stimulus, so Naka–Rushton fits were poorly constrained. We estimated the S-cone gain in these cells instead as the response to the highest contrast S-cone stimulus divided by the S-cone contrast of that stimulus. The average S-cone gain of PC ($n = 102$) and MC ($n = 16$) cells calculated in this manner was 0.06 imp s^{-1} %$^{-1}$ and 0.13 imp s^{-1} %$^{-1}$, respectively (see also Szmajda *et al.* 2006). The achromatic contrast gain of blue-on (mean = 0.45 imp s^{-1} %$^{-1}$) and blue-off (0.17 imp s^{-1} %$^{-1}$) cells is lower than that of PC (0.83 imp s^{-1} %$^{-1}$) and MC cells (2.89 imp s^{-1} %$^{-1}$). The contrast threshold apparent in some blue-off cells will cause us to slightly underestimate the slope of the rising portion of their contrast response function (as in Fig. 1D).

Another measure of the contrast sensitivity of a neuron is the *integrated sensitivity* (Croner & Kaplan, 1995), which is estimated directly from the parameters of the DOG model. The integrated sensitivity is calculated as the product of the centre sensitivity and the square of the centre radius: $K_c \pi r_c^2$. In Fig. 3D we have plotted centre sensitivity against centre radius. Parameters were estimated from S-cone gratings in blue-on and blue-off cells, and from achromatic gratings in PC and MC cells. The data points for all cells fall on descending diagonal lines, indicating that for all cells of a given class, integrated sensitivity is approximately constant across the retina. The data points for blue-on cells fall slightly above those for PC cells, indicating that the integrated sensitivity of blue-on cells for S-cone gratings (geometric mean = 0.71 imp s^{-1} %$^{-1}$, $n = 55$) is higher than that of PC cells for achromatic gratings (0.39 imp s^{-1} %$^{-1}$, $n = 182$). The integrated sensitivity of blue-off cells for S-cone gratings (0.28 imp s^{-1} %$^{-1}$, $n = 15$) is lower than that of blue-on cells. A regression fit to the log-transformed data for blue-off cells has a lower elevation than the fit for blue-on cells ($P < 0.01$), indicating that the difference is not simply attributable to the larger receptive field diameter of blue-off cells.

Our estimate of the integrated sensitivity of MC cells for achromatic gratings (0.65 imp s^{-1} %$^{-1}$, $n = 30$) is likely to be an underestimate, given the high contrast used (mean = 85%). At this contrast, the responses of MC cells have begun to saturate. Saturation, albeit weaker, is likely also the cause of the discrepancy between the contrast sensitivity of PC cells estimated from the Naka–Rushton and DOG fits. Relative to S-cone gratings, blue on and blue off cells are less sensitive to achromatic gratings (integrated sensitivities are 0.24 ($n = 36$), and 0.20 ($n = 13$) imp s^{-1} %$^{-1}$, respectively; data not shown).

Figure 4. Spatial structure of the S- and ML-cone receptive fields of blue-on and blue-off cells

A, spatial frequency tuning of an example blue-on cell for S-cone selective (circles) and ML-cone selective (open squares) gratings. Smooth curves show fits of the DOG function defined in Methods. *B*, comparison of the radius of the ML-cone mechanism *versus* that of the S-cone mechanism in the 11 blue-on cells (triangles) and one blue-off cell (filled circle) from which we obtained these measurements. The arrow identifies the cell shown in A.
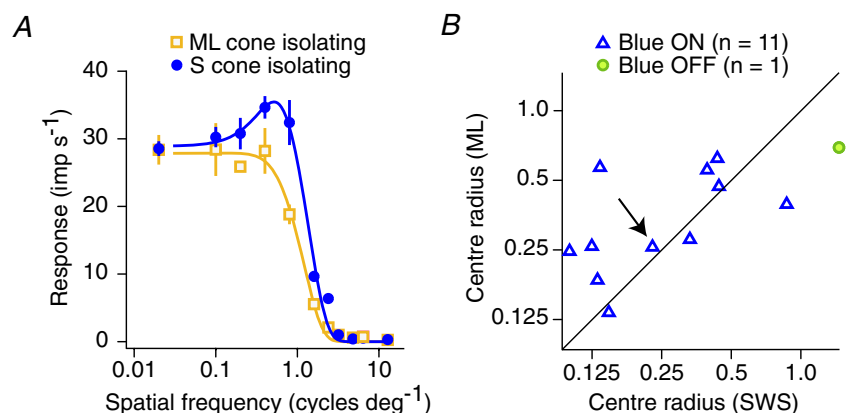
Cone inputs and chromatic selectivity

The contrast gain data suggest that blue-on and blue-off cells are specialized for signalling the activity of the S-cones. We were interested to know the weight and sign of S-cone input into these cells relative to any input they might also receive from ML-cones. We estimated the S-cone weight using the colour circle (Sun *et al.* 2006*a*) and colour vector (Hashemi-Nezhad *et al.* 2008) stimulus sets, described in Methods. Example responses to the colour circle stimulus are shown for a blue-on cell in Fig. 5. The stimulus is sketched in Fig. 5*A*. Responses to counter-clockwise (CCW, black bars) and clockwise (CW, grey bars) modulation at 1, 2, 4, 8 and 16 Hz are shown in Fig. 5*B*. The *x*-axis shows stimulus angle, the *y*-axis shows response amplitude. In order to facilitate comparison of the PSTHs in response to CW and CCW modulations we have inverted the histogram for CW modulation.

In Fig. 5*C* response phase for CW (open symbols) and CCW (filled symbols) modulations is plotted against temporal frequency. The rate of change of phase with temporal frequency is determined primarily by the visual latency of the cell, and the *y*-intercept defines the relative signed weight of S- and ML-cone input to the receptive field. For the example blue-on cell the *y*-intercept is 141.5 deg, corresponding to an S weight of 0.44 and an ML weight of −0.56, respectively,

Figure 6*A* shows the histogram of the normalized weight of S-cone input for all PC ($n = 89$), MC ($n = 18$), blue-on ($n = 15$) and blue-off cells ($n = 6$) in our sample. The inset graph shows S-cone weights for those cells ($n = 25$) which were measured using both the colour circle and the colour vector stimulus sets. There is good correspondence of S-cone weights measured with the different methods (correlation coefficient 0.95, $r^2 = 0.91$), so the data were pooled for further analysis.
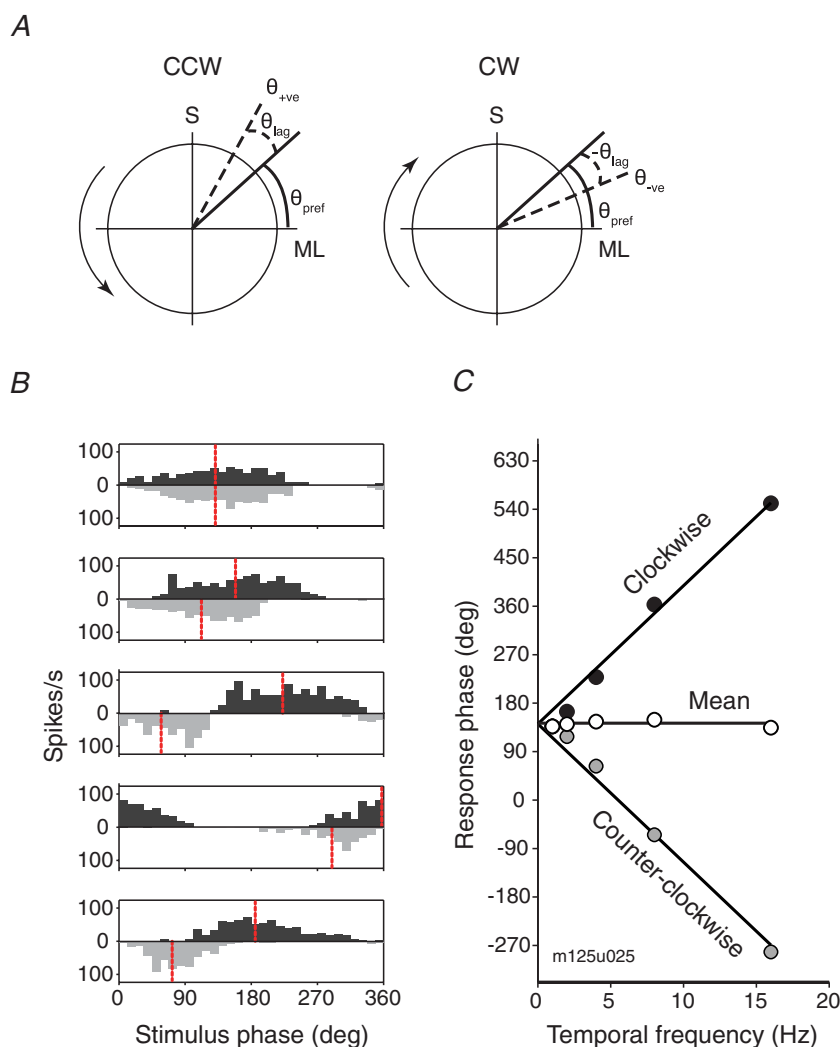

Figure 5. Measuring cone inputs to LGN neurons

A, cells are presented with a spatially uniform field, the chromaticity of which is modulated around a colour circle in clockwise (positive temporal frequencies) or counter-clockwise (negative temporal frequencies) directions within an S- *versus* ML-cone plane. For the two directions of modulation the preferred vector (θ_{pref}) of a linear neuron does not change, but the phase delay (θ_{lag}) changes sign. Averaging response phase for the two directions of modulation cancels θ_{lag} to reveal the cell's preferred vector θ_{pref} in the stimulus plane, and hence the relative weight of cone input. *B*, peri-stimulus time histograms (PSTHs), folded to one cycle of modulation, collected at different temporal frequencies (from top to bottom: ±1, ±2, ±4, ±8 and ±16 Hz). Responses to positive temporal frequencies are shown as black bars; responses to negative temporal frequencies are shown as grey bars (inverted to facilitate comparison). In each panel the vertical dashed lines show the peak phase of the first harmonic recovered from Fourier analysis of the PSTHs. *C*, response phase as a function of temporal frequency. Black symbols show positive temporal frequencies; grey symbols show negative temporal frequencies; open symbols show their average. Straight lines show the result of a regression analysis of response phase *versus* temporal frequency. The *y*-intercept identifies the preferred colour vector.

As in previous studies of ganglion cells in macaque retina (Sun *et al.* 2006*a*,*b*) and relay cells in marmoset LGN (Hashemi-Nezhad *et al.* 2008), we found only very weak S-cone inputs to PC cells (mean -0.010, S.D. 0.091, $n = 89$) or MC cells (mean -0.006, S.D. 0.091, $n = 18$). In Fig. 6*B* we have separated the PC cells into on- and off-subpopulations. This shows that the S-cone input to on-centre PC cells tends to have negative weight (mean -0.045, S.D. 0.054, $n = 50$) whereas the input to off-centre cells tends to have positive weight (mean 0.033, S.D. 0.054, $n = 39$, $P < 0.02$, Wilcoxon's rank-sum test).

Figure 6 indicates that S-cone input into PC cells is very weak, suggesting that these cells show a bias against S-cones. Another way of addressing this question is to ask whether the observed S-cone input is less than that we would expect by chance, given the relative density of S- and ML-cones across the retina (Sun *et al.* 2006*b*; Hashemi-Nezhad *et al.* 2008). In Fig. 7 we compare the measured S-cone weights with a simple prediction based
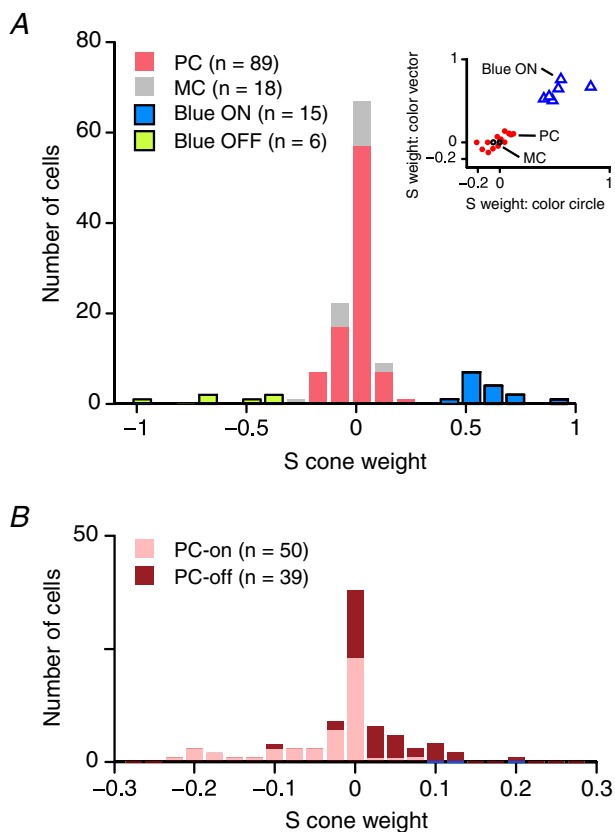

Figure 6. Weight of S cone inputs to geniculate cells
A, histogram of normalized S-cone weights. Pooled results from measurements using the 'colour circle' and 'colour vector' methods are shown. Mean values: PC, -0.010; MC, -0.006; blue-on, 0.612, blue-off, -0.588. The inset graph compares S-cone weight for cells studied using both methods. *B*, the inputs to PC cells shown at a finer scale. Note that S-cone weights have the opposite sign to the centre weight for both on-centre and off-centre cells.
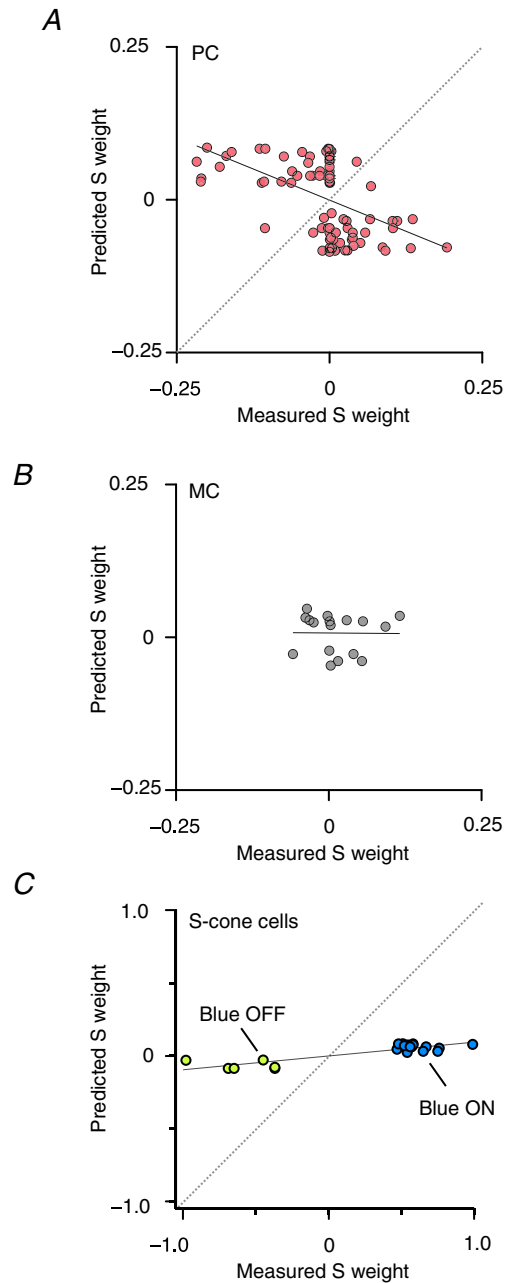

Figure 7. Comparison of measured S-cone weight with predictions based on random connections to the cone mosaic
A, parvocellular (PC) cells. *B*, magnocellular (MC) cells. *C*, blue-on and blue-off cells. The *x*-axis on each graph shows the S-cone weight estimated using the colour circle or colour vector methods. The *y*-axis shows the prediction for random connections, that is the proportion of S-cones at the receptive field eccentricity of the recorded cell. Predicted weights are signed positive for on-centre cells and negative for off-centre cells. Grey lines show linear regressions: PC, $y = -0.0006 - 0.408x$, $r^2 = 0.27$, $n = 88$; MC, $y = -0.0068 - 0.0080x$, $r^2 < 0.01$, $n = 17$; blue-on and blue-off, $y = 0 + 0.0946x$, $r^2 = 0.76$, $n = 21$. Note the different scale in panel C, consistent with much stronger input to blue-on and blue-off cells than to PC and MC cells.
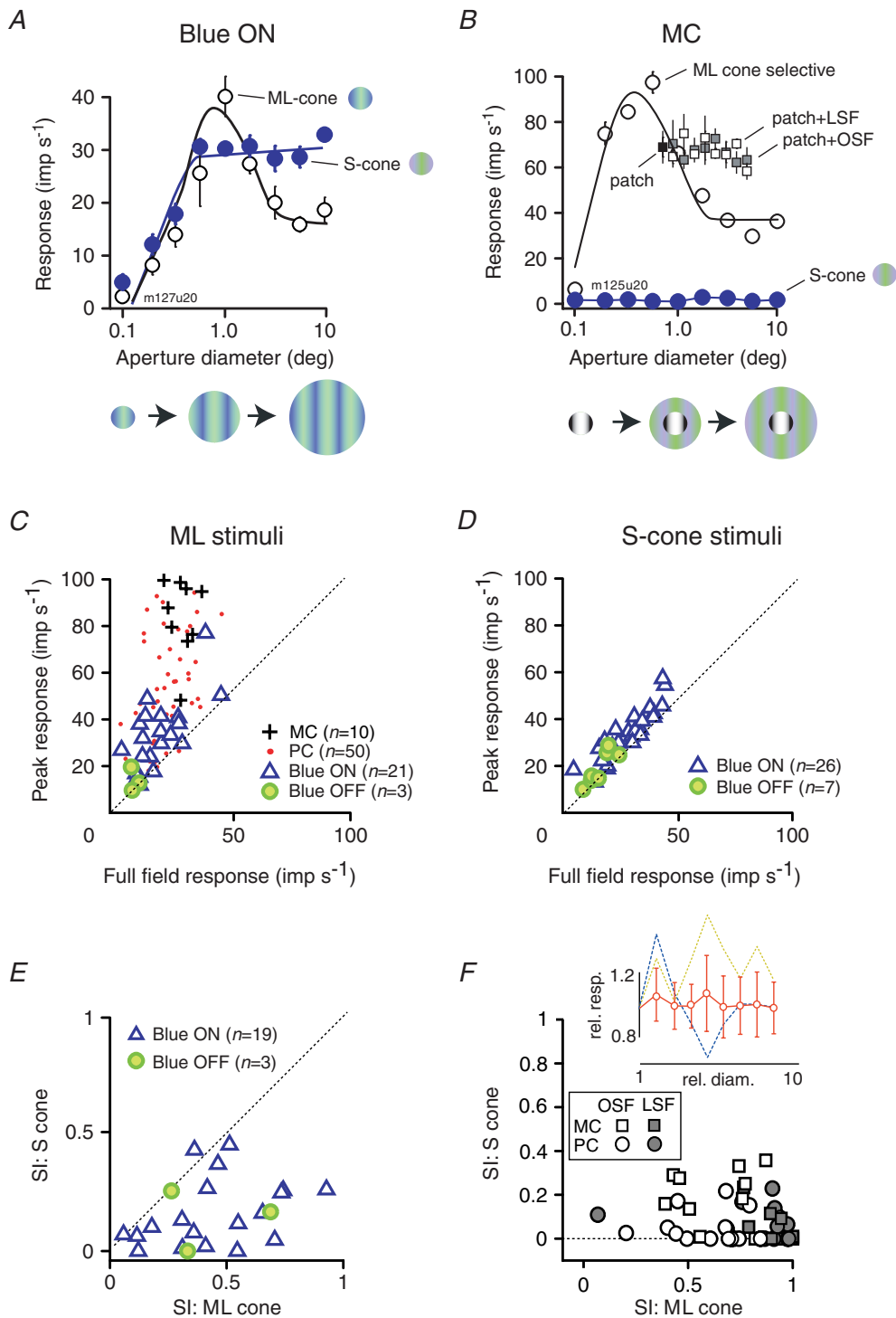
Figure 8. Extra-classical inhibition (surround suppression) in different classes of LGN neuron
A, responses of a blue-on cell to optimum spatial frequency gratings as a function of aperture radius (icons show approximate stimulus configurations). Filled symbols show responses to S-cone selective gratings; open symbols show responses to ML selective gratings. *B*, same as *A*, but for an MC cell. Also shown is the response to a small patch of achromatic (M + l + S) grating presented either alone (filled square), or overlaid on a grating that modulated only the S-cones (grey squares: uniform field; open squares: preferred achromatic spatial frequency). The stimulus is sketched beneath the graph. *C*, response to the preferred aperture diameter *versus* response to the largest aperture tested (10° diameter) for PC cells (points), MC cells (+), blue-on cells (triangles) and blue-off cells (filled circles). Stimuli were drifting achromatic or ML-cone selective gratings. *D*, response to S-cone selective

on the proportion of S-cones at the same receptive field eccentricity. The analysis is consistent with that used in our previous study (Hashemi-Nezhad *et al.* 2008) but the datasets are non-overlapping, and here we additionally consider the sign of S-cone input. The majority of receptive fields was recorded outside the fovea, where there is numerical convergence of cone and cone bipolar inputs to PC cells (Goodchild *et al.* 1996). Accordingly the predicted S-cone weight (Fig. 7) has been given a positive sign for on-centre cells, and a negative sign for off-centre cells. The PC cells (Fig. 7*A*) form two clusters corresponding to the on- and off-centre response types. Overall there is a weak negative correlation between predicted and measured S-cone weight (correlation coefficient: -0.52, $r^2 = 0.27$). This indicates that where present the S-cone contribution to cell responses tends to be antagonistic to the centre mechanism. Correlation was insignificant (-0.01, $r^2 < 0.01$) for MC cells (Fig. 7*B*) and, as expected, was very strong for blue-on and blue-off cells (0.87, $r^2 = 0.76$). In summary, the data are consistent with weak S-cone input to the receptive field surround of some PC cells, but on average the strength of S-cone input to PC and MC cells is below that predicted by random connections to the S-cone mosaic.

Extra-classical receptive field properties

The visually evoked responses of marmoset PC, KC and MC neurons can be suppressed by stimuli positioned outside the classical receptive field (extraclassical inhibition (ECI); Solomon *et al.* 2002). The specificity of cone signals contributing to extraclassical inhibition is not known. We therefore determined the cone selectivity of extraclassical inhibition in blue-on, blue-off, PC and MC cells. We measured diameter-tuning curves for S-cone selective and achromatic (or, for some cells, ML-cone selective) gratings, using spatial frequencies at or slightly above the preferred spatial frequency for each colour direction. This ensures that any suppression observed at large stimulus diameters cannot be due to the action of the classical receptive field surround (Sceniak *et al.* 1999; Solomon *et al.* 2002; Einevoll & Plesser, 2005).

Example responses from a blue-on cell are shown in Fig. 8*A*. For this cell the response to a high frequency

ML-cone selective grating increases with aperture size to about 1 deg diameter, as the classical receptive field centre mechanism is recruited. Responses to larger diameters are reduced by the extraclassical suppressive mechanism. When S-cone selective gratings are used, however (filled symbols, Fig. 8*A*), the diameter-tuning curve rises rapidly with increasing diameter to about 1 deg, then more slowly for larger stimuli. This indicates that ML-cones, but not S-cones, contribute to extraclassical inhibition in the blue-on cell.

Figure 8*B* shows the responses of an MC cell. Response to ML gratings decreases beyond the preferred stimulus diameter, as previously shown (Solomon *et al.* 2002). The MC cell does not show overt responses to the S-cone stimulus (Fig. 8*B*), but it is nevertheless possible that S-cones could exert suppressive effects on visually evoked responses. We therefore tested for S-cone driven extraclassical inhibition by embedding a small patch of optimally sized achromatic grating (of non-saturating contrast) in the large (10 deg) field of S-cone selective grating. If S-cones contribute to extraclassical suppression then the response evoked by the achromatic patch should decrease as the diameter of the S-cone stimulus is increased. Figure 8*B* shows recordings from an example cell: the black square shows the response to the achromatic patch alone, and the open and filled squares show response as the outer diameter of an annulus of S-cone stimulus is increased. It can be seen that S-cone modulation has no suppressive effect on the response to the patch of achromatic grating.

The responses shown in Fig. 8*A* and *B* were typical for the cells in our dataset. Population data are shown in Fig. 8*C–F*. In Fig. 8*C* we compare the response evoked at the optimum diameter to the response evoked at the largest diameter tested (referred to here as 'full-field'). No systematic differences were seen on comparing responses to ML-cone isolating and achromatic gratings, so the data were pooled for this analysis. All of the symbols lie above the diagonal, confirming the presence of extraclassical inhibition in all LGN cell classes (Solomon *et al.* 2002). Figure 8*D* plots, using the same format as in Fig. 8*C*, data recorded from blue-on and blue-off cells in response to S-cone gratings. The cloud of data points is displaced only slightly above the unity line, in other words, the

gratings of the preferred aperture diameter compared to response to the largest aperture tested (10 deg diameter) for blue-on cells (triangles) and blue-off cells (filled circles). *E*, suppression index (SI) for S-cone selective gratings compared to SI for achromatic or ML-cone isolating gratings. Triangles, blue-on cells; filled circles, blue-off cells. *F*, the SI for S-cone selective gratings plus achromatic patch, compared to SI for achromatic or ML-cone isolating grating. Circles, PC cells; squares, MC cells; open symbols, gratings at the optimal spatial frequency (OSF); grey symbols, temporally modulated uniform fields ('low' spatial frequency; LSF). Mean SIs for PC cells: S-cone uniform field = 0.06, S-cone grating = 0.05, ML-cone uniform field = 0.82, ML-cone grating = 0.6. Mean SIs for MC cells: S-cone uniform field = 0.05, S-cone grating = 0.19, ML-cone uniform field = 0.91, ML-cone grating = 0.63. The inset graph shows mean and standard deviation of these cells as a function of the S-cone selective annulus diameter. Dashed lines show values for two cells showing substantial deviation from the population mean.

full-field grating has only weak suppressive effects on blue-on and blue-off cells. This implies that the S-cones do not contribute to extraclassical inhibition to an extent greater than expected on the basis of random connection.

We quantified the strength of surround suppression by calculating a suppression index (SI): 1 − (full field response/peak response). This index takes values near 0 if response is not attenuated by full-field stimuli, and a value of 1 if full-field stimuli completely abolish the response. As previously shown (Solomon et al. 2002) suppression is stronger in MC cells (mean SI = 0.68, $n = 10$) than in PC cells (0.52, $n = 50$). Additionally, suppression comparable to PC cells is present in blue-on and blue-off cells (mean SIs of 0.45, $n = 21$, and 0.43, $n = 3$; see also Solomon et al. 2002).

Mean suppression indices for blue-on and blue-off cells were substantially lower for S-cone selective stimuli (blue-on, 0.20; blue-off, 0.19) than for achromatic stimuli. Consistently, for the cells in which we have both measurements, the SI for achromatic gratings is greater than for S-cone gratings (Fig. 8E), especially among those cells which are strongly suppressed by achromatic stimuli. These results confirm what is implied by Fig. 8D, that is, the S-cones contribute less than ML-cones to surround suppression in blue-on and blue-off cells.

In Fig. 8F we show population data for MC and PC cells, obtained using the approach shown in Fig. 8B. Here the suppression index for ML-cone selective gratings is compared to the effect of a large annulus of S-cone stimulus surrounding an optimal sized achromatic patch (0 indicates no reduction of response, 1 indicates that response is completely abolished). Open symbols show values derived from temporal modulation of uniform S-cone fields, and filled symbols show values for gratings of preferred frequency. All data points lie below the unity line, in other words, for all PC and MC cells tested modulation of S-cones has little or no suppressive effect on visually evoked responses. The PC cells were almost completely unaffected by S-cone modulation in the surround (mean SI: preferred SF = 0.05, uniform field = 0.06, $n = 14$; compared with 0.52 for ML stimuli). An annulus of S-cone grating of preferred spatial frequency evoked some suppression in MC cells (mean SI = 0.2, $n = 10$), but this was always much weaker than suppression evoked by ML-cones (mean SI = 0.63). The cone contrast for both S and ML stimuli was ∼60%, so the weaker ECI observed with S-cone stimuli is not due simply to a contrast imbalance between the two conditions. No clear difference in receptive field size, peak response rate or visual field eccentricity was apparent when cells showing relatively high (> 0.2) SI were compared to cells with weaker SIs ($P > 0.05$, ANOVA).

The inset graph in Fig. 8F shows mean and standard deviation of response amplitude for these cells as a function of the S-cone selective annulus diameter. No

systematic variation is apparent. Consistently, the mean slope of the annulus area–response amplitude regression lines for the cells shown in Fig. 8F (mean, −0.003; S.D. 0.025, $n = 24$) is not significantly different from zero ($P = 0.57$, t test). We did, however, find substantial variability between and within cells (two extreme examples are shown with dashed lines in the inset, Fig. 8F). It is feasible that such variation results from weak 'patches' of S-cone input to ECI, analogous to those demonstrated for achromatic stimuli (Webb et al. 2005), but we did not explore this possibility further.

Collectively, these data demonstrate that ECI is present in all cell classes (PC, MC, blue-on, and blue-off), and the input into the ECI in all classes comes principally from ML-cones. On the basis of the signal : noise ratio of our data we cannot, however, rule out the possibility that S-cones contribute to ECI at a level consistent with random sampling from the cone mosaic.

Real and spurious S-cone responses in MC and PC cells

A small number of PC (5 of 195) and MC (2 of 22) cells in our sample showed robust responses (> 10 imp s⁻¹) to our nominal S-cone selective stimuli. Does this constitute true S-cone input into these cells, or is it simply due to residual ML-cone activation ('bleed-through') evoked by our ostensibly S-cone selective stimulus?

We addressed this question by comparing the pattern of responses to S-cone selective and achromatic gratings. Figure 9A shows the 'low end' of the achromatic contrast response functions in dichromatic MC cells (open symbols). In the absence of S-cone input the responses in dichromatic animals must be driven by the single remaining (ML) cone type. The response to S-cone selective gratings (filled symbols) superimposes on the achromatic contrast response function (open symbols) when the contrast axis is rescaled by a factor of 0.075. This is consistent with our calculation that our highest contrast S-cone stimulus produces ∼5% ML-cone contrast (0.075 times ∼66% maximum S-cone contrast). Because the S-cones are present at a lower spatial density, and form a sampling matrix independent of the ML-cones, the spatial frequency transfer characteristics of putative S-cone inputs should be quite different from that of ML-cone inputs. However, we found the spatial frequency tuning functions for the ML selective and S-cone selective stimulus conditions can be made to superimpose, by scaling the response to S-cone selective gratings (Fig. 9B). Figure 9C–F shows data in the same format, averaged across all MC cells (Fig. 9C and D) and PC cells (Fig. 9E and F). In all cases the scaled S-cone tuning curves resemble those measured with achromatic gratings.

We did encounter a small number of PC cells which showed more definite signs of S-cone input. The PC

cell shown in Fig. 10*A* was encountered near the bottom of the internal PC layer; the receptive field eccentricity was ∼2.5 deg. Figure 10*A* shows spatial frequency tuning curves for achromatic and S-cone selective stimuli. Unlike the majority of PC cells, this cell responds to low spatial frequency S-cone selective gratings. The inset panel (Fig. 10*A*) shows the PSTH for this cell in response to a low spatial frequency S-cone selective stimulus (0.1 cycle deg^{-1}). The discharge peak is close to the response phase of blue-off cells for the same stimulus (compare with Fig. 1*C*), indicating that the S-input is inhibitory (i.e. sign-inverting). A conventional PC cell

with a neighbouring receptive field was encountered ∼330 μm above this cell (Fig. 10*B*). It showed no response to S-cone selective gratings, thus ruling out spurious ML contrast as the source of the responses shown in Fig. 10*A*.

Tailby *et al.* (2008) reported some S-cone recipient cells in macaque LGN that receive weak (∼20%) inhibitory S-cone inputs, but otherwise resemble PC cells. The responses shown in Fig. 10*A* are consistent with that result. However, by our criteria this cell was not classified as blue-off, because the peak response to S-cone selective gratings was below 10 imp s^{-1}, and it was more sensitive to achromatic modulation than to S-cone modulation.
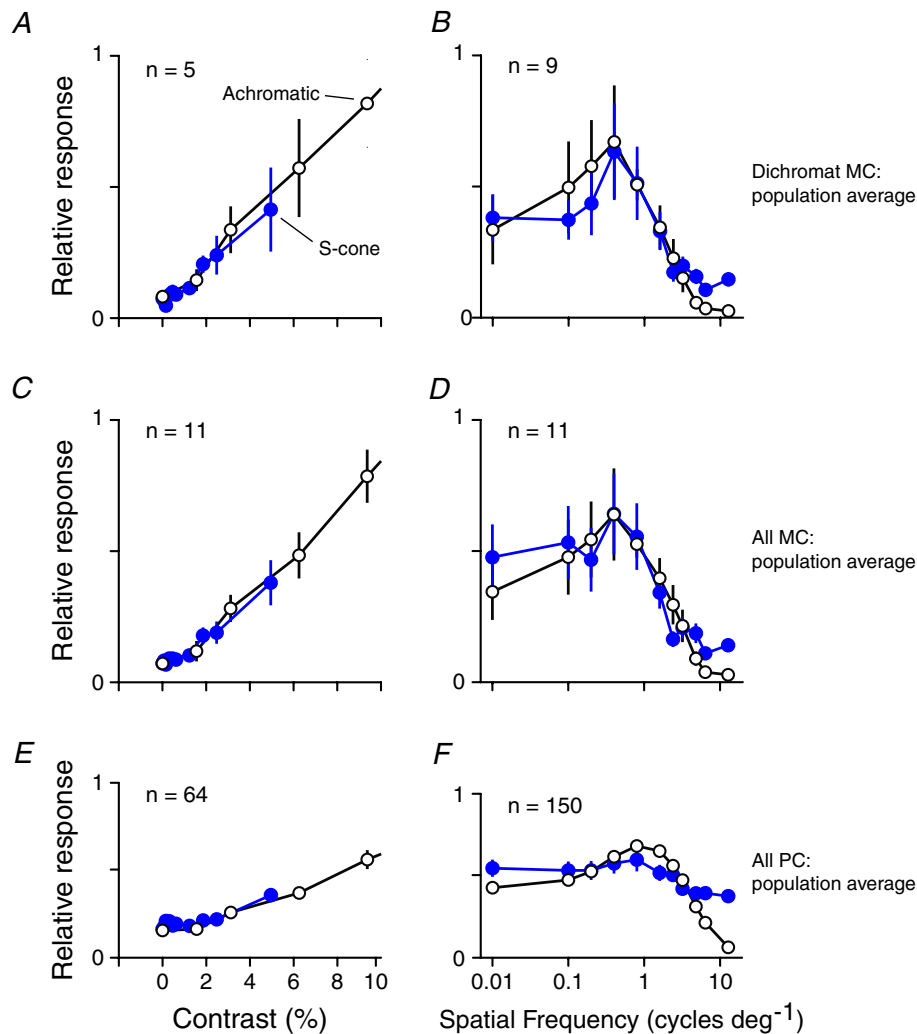

Figure 9. MC and PC cell responses to S-cone selective gratings attributable to residual ML-cone contrast
A, average contrast response of MC cells for achromatic gratings (open symbols), and for S-cone selective gratings after scaling S-cone contrast by a factor of 0.075. The population average includes only data obtained from neurons encountered in dichromatic animals. *B*, population average spatial frequency tuning function of MC cells for achromatic gratings (open symbols), and for S-cone selective gratings after scaling S-cone contrast by a factor of 5. The population average includes only data obtained from neurons encountered in dichromatic animals. *C* and *D*, same as *A* and *B* but for MC cells encountered in dichromatic and trichromatic animals. *E* and *F*, same as *A* and *B* but for PC cells encountered in dichromatic and trichromatic animals.

A final illustration of the difference between real and spurious signs of S-cone input is shown in Fig. 10*C*–*F*. This MC cell was recorded at 14 deg eccentricity. The cell shows typical spatial and contrast tuning for achromatic gratings (open symbols, Fig. 10*C* and *D*), and negligible responses to S-cone selective gratings (filled symbols, Fig. 10*C* and *D*). Following these recordings we reconfigured the visual stimulus generator to use cone nomograms incorporating absorption by macular pigment. Under this 'foveal' stimulus configuration (Fig. 10*E* and *F*) the cell responds vigorously to the nominally S-cone isolating stimulus. As expected (data not shown) this spurious sign of S-cone input disappeared when the stimulus was re-calibrated using nomograms appropriate for this visual field location.

Taken together, the results shown in Figs 7, 9 and 10 show that most MC and PC cells receive negligible input from S-cones, that is, the S-cone functional input is substantially lower than predicted by random connections to the cone mosaic. Surprisingly, signs of S-cone inputs to

MC cells are less convincing than are signs of S-cone input to a minority of PC cells.

Discussion

Distinct spatial properties of blue-on and blue-off cells

The distinction between on- and off-centre neurons constitutes a fundamental dichotomy of the subcortical visual system. While there are subtle differences between on- and off-centre PC and MC neurons (Fig. 3 herein; Dacey & Petersen, 1992; Lankheet *et al.* 1998; Chichilnisky & Kalmar, 2002), within each of these cell classes the opposite polarity 'channels' are largely functional complements of one another. The data presented here and in Szmajda *et al.* (2006), together with recent recordings from macaque LGN (Tailby *et al.* 2008) reveal that relative to blue-on cells, blue-off cells have larger receptive fields, weaker spatial opponency, lower contrast
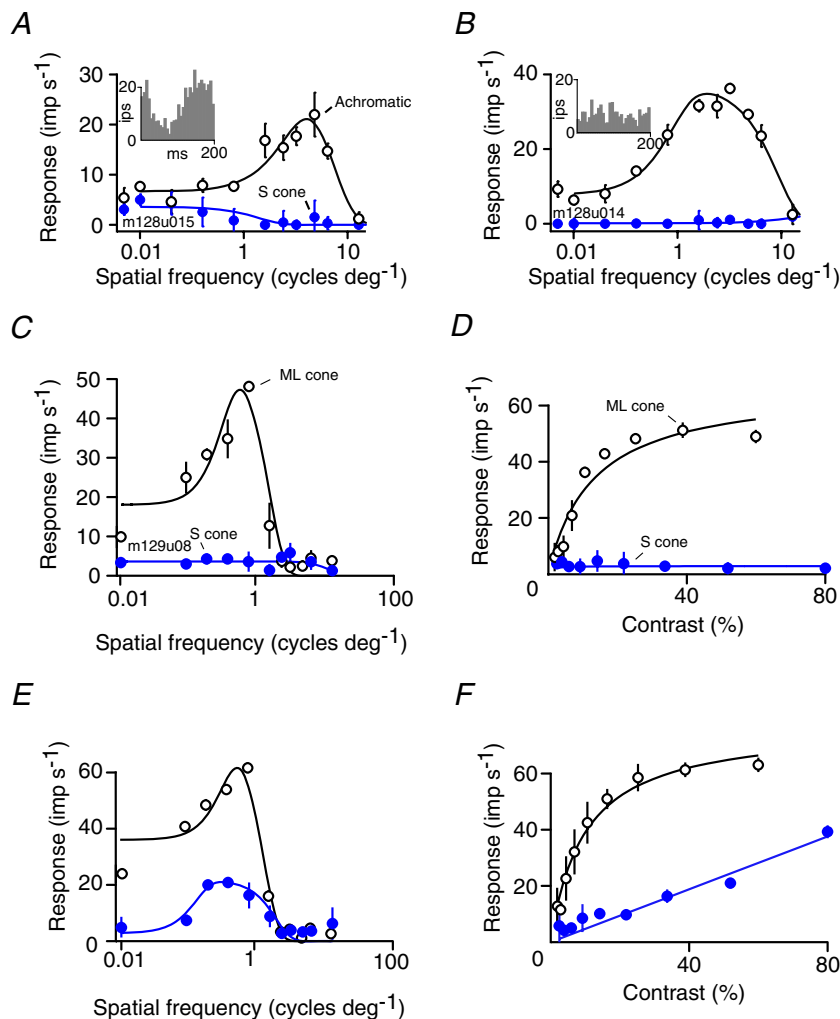
Figure 10. Real and spurious S cone inputs to geniculate cells
A, responses of a cell recorded near the bottom of the internal PC layer to achromatic (open symbols) and S-cone selective gratings (filled symbols). Smooth curves show the best fitting difference of Gaussians function. The inset graph shows a PSTH for this cell in response to a 0.1 cycle deg^{-1} S-cone selective grating (folded to one cycle of modulation). *B*, same as *A*, recorded from a cell encountered within the internal PC layer ~330 μm above the cell shown in *A*. *C*–*F*, demonstration of spurious responses to S-cone selective gratings. Spatial frequency (*C* and *E*) and contrast tuning functions (*D* and *F*) are shown for an MC cell (receptive field eccentricity 14 deg). In *C* and *D* the stimulus chromaticity was calculated without incorporating absorption by macular pigment. Note the lack of response to S-cone selective gratings (filled symbols). In *E* and *F* the stimulus chromaticity was calculated assuming absorption by macular pigment. Note the response to the nominally S-cone selective stimulus.

sensitivity, lower overall responsivity, and longer visual response latencies than blue-on cells. These asymmetries are more pronounced than those observed between on- and off-centre PC or MC cells. (Fig. 3*C*; see also Lankheet *et al.* 1998; Solomon & Lennie, 2005; Szmajda *et al.* 2006; Tailby *et al.* 2008). These results are consistent with psychophysical evidence that points to poorer spatial precision and contrast sensitivity decrement-mediated *versus* increment-mediated detection of S-cone contrast (McLellan & Eskew, 2000; Racheva & Vassilev, 2008; Zlatkova *et al.* 2008).

As expected from recordings from blue-on cells in macaque retina (Solomon *et al.* 2005; Field *et al.* 2007) we found the diameter of the S-cone field of blue-on cells in marmoset LGN is slightly smaller than the ML-cone field (by a factor of 0.75, Fig. 4*B*). This is consistent with other evidence that the ML-cone field arises from lateral inhibitory inputs from horizontal cells in the outer plexiform layer (Dacey *et al.* 1996, 2005; Solomon *et al.* 2005; Field *et al.* 2007). However, blue-on cells often show spatial offset between S and ML subfields (Field *et al.* 2007), and some blue-on cells show orientation- and direction-tuning for achromatic gratings (Forte *et al.* 2005; Tailby *et al.* 2008). These features are more consistent with the asymmetric dendritic field arrangement of small bistratified cells. As discussed below, these alternative possibilities are not mutually exclusive.

There are two main factors which could influence the spatial frequency measurements reported here. The first is chromatic aberration. Refractions in optic media are wavelength dependent, so the retinal image is only in focus for a narrow range of wavelengths. This means that the spatio-chromatic properties of cells that draw on S- as well as ML-cones will necessarily vary with the refractive state of the eye. In our experiments the eye's refraction was optimized for the ML-cones in order to give measurements consistent with natural viewing by an emmetropic eye. Under these conditions, high-frequency spatial contrast at short wavelengths is attenuated (Marimont & Wandell, 1994; McLellan *et al.* 2002); in other words the full resolving power of the S-cone array is not available to blue-on and blue-off cells. This could be the reason why, for these cells, the receptive field radius estimated from S-cone gratings was consistently slightly larger than that for achromatic gratings (see Results). A second factor concerns the difference-of-Gaussians model used to estimate receptive field dimensions. Data from our laboratory (Forte *et al.* 2005; Hashemi-Nezhad *et al.* 2008) and others (Chichilnisky & Baylor, 1999; Reid & Shapley, 2002; Field *et al.* 2007; Tailby *et al.* 2008) indicates that the ON and OFF subfields in blue-on and blue-off cells can be offset from one another in both space and time. Such asymmetries mean that receptive field dimensions can be influenced by the orientation, direction and temporal frequency of the stimulus. In summary,

the centre radius measures reported are best considered as a single 'slice' through a receptive field which can be substantially more complex than the canonical 'Type II' organization originally proposed (Wiesel & Hubel, 1966). We are currently exploring a more complete description of the receptive fields of blue-on and blue-off cells.

Neural pathways feeding blue-on and blue-off cells

Most anatomical studies to date have identified a single type of 'blue-cone bipolar cell' that is specialized for drawing input from S-cones (Kouyama & Marshak, 1992; Ghosh *et al.* 1997; Lee & Grünert, 2007). A small bistratified ganglion cell has been identified as the anatomical substrate of the functionally characterized blue-on cell (Dacey & Lee, 1994), but the functional significance of the bistratified dendritic tree of these cells remains unclear. The inner dendritic tier of the small bistratified cell is costratified with the terminals of blue-cone bipolar cells to give a source of on-type excitation from S-cones (Kouyama & Marshak, 1992; Calkins *et al.* 1998; Ghosh & Grünert, 1999). There is evidence that the S *versus* ML opponency observed in blue-on cells is inherited from the blue-cone bipolar cell (Field *et al.* 2007), but antagonistic input from ML-cones could also arise *via* bipolar inputs onto the outer tier of small bistratified cells (Calkins *et al.* 1998; Ghosh & Grünert, 1999). More than one class of large, sparsely branching ganglion cell is likely to carry S-off signals (Dacey & Packer, 2003; Dacey *et al.* 2003, 2005). These cells also costratify with the terminals of blue-on bipolar cells (Dacey *et al.* 2003, 2005; Szmajda *et al.* 2008) but the required sign-inverting synaptic circuits have not been characterized. The more low-pass spatial tuning in blue-off cells (compared to blue-on cells) could be a result of spatial pooling of bipolar inputs, whereby the effect of bipolar surrounds would only be manifest at the 'edge' of the spatial pool.

An alternative source of S-off signals is suggested by anatomical evidence from macaque that S-cones contribute to off-type midget-parvocellular pathway bipolar cells (Klug *et al.* 2003). However, our data (Figs 2 and 3) and recordings from macaque LGN (Tailby *et al.* 2008) show that blue-off cells have the largest receptive fields at any given eccentricity. It does remain possible that there is convergence of S-off cone signals at the level of the LGN or that the connections identified by Klug *et al.* (2003) are specific to the macaque fovea.

Classical and extraclassical inhibition in S-cone pathways

Two main features of our data show that the S-cones exert little suppressive effect on visual signal transmission

through the LGN. Firstly, the spatial frequency tuning curves of blue-on and blue-off cells are only weakly bandpass. On average, the low frequency attenuation (response to a 0.01 cycle deg^{-1} grating divided by the response to a grating of preferred spatial frequency) for S-cone isolating gratings was 0.69 for blue-on cells and 0.89 for blue-off cells. This compares with 0.53 for PC cells and 0.56 for MC cells (measured with achromatic gratings). Secondly, S-cones provide little input to the mechanism that drives suppression from the extraclassical receptive field. Whereas all cell types were suppressed by the ML-cone contrast outside the classical receptive field (mean suppression indices: MC, 0.68; PC, 0.52; blue-on, 0.45; blue-off, 0.43), there was little evidence of

suppression by S-cone contrast in the same regions (MC, 0.20; PC, 0.06; blue-on, 0.20; blue-off, 0.19, respectively; see Fig. 8). This is also consistent with evidence that colour-selective neurons in V1 are relatively immune to extraclassical suppression by chromatic stimuli (Ts'o & Gilbert, 1988; Solomon et al. 2004). Thus ML-cone signals contribute to suppression in all cell classes, irrespective of the cone type that dominates the classical receptive field.

S-cone input to PC and MC cells

Our results present further evidence that the bias against S-cone inputs, which is present in PC and MC pathway ganglion cells (Sun et al. 2006a,b), is largely preserved in the LGN (see also Hashemi-Nezhad et al. 2008). Three main lines of evidence support this conclusion. Firstly, on average the PC and MC cells show little or no response to high-contrast S-cone selective stimuli at any spatial frequency (Fig. 2). Secondly, responses to S-cone selective stimuli are well accounted for by a rescaling of the responses to achromatic stimuli (Fig. 9). Thirdly, two methods for estimating functional weight of S-cone inputs give distributions which are centred close to zero mean S-cone weight for the MC and PC populations (Figs 5–7).

Figure 11A–D compares the distribution of S-cone weights for PC and MC cells in the macaque retina (Fig. 11A and C; data from Sun et al. 2006b) with the distributions obtained in the present study for marmoset LGN (Fig. 11B and D). Although all these distributions are distributed around zero mean, the variance is greater for the LGN data; specifically the distribution for PC cells has long 'tails', with a small number of PC cells showing more than 5% input from S-cones. In marmoset retina a small proportion (~25%) of off-midget bipolar cells receive sparse contacts from S-cones (Lee et al. 2005). However, these contacts most likely involve ionotropic (AMPA) glutamate receptors, and thus would yield the same functional sign as input from ML-cones (Puller et al. 2007). Cross-talk from retinal or geniculate interneurones is a possible alternative source of inhibitory S-cone inputs. Additional data on prereceptoral absorbance in marmoset eye may also reduce a possible source of inaccuracy in our cone weight calculations.

Figure 11E shows S-cone weights reported for MC cells in macaque by Chatterjee & Callaway (2002). The distribution is centred close to 9% S-cone weight, which is clearly different from the mean values for MC cells in marmoset LGN (mean = −0.6%, Fig. 11D) or MC ganglion cells in macaque (< 1%, Fig. 11C, data from Sun et al. 2006b). Part of the discrepancy may be due to methodological differences. The recordings in all three studies were made predominantly from receptive fields above 2 deg eccentricity, but in Chatterjee & Callaway's experiments the stimuli were calculated using foveal
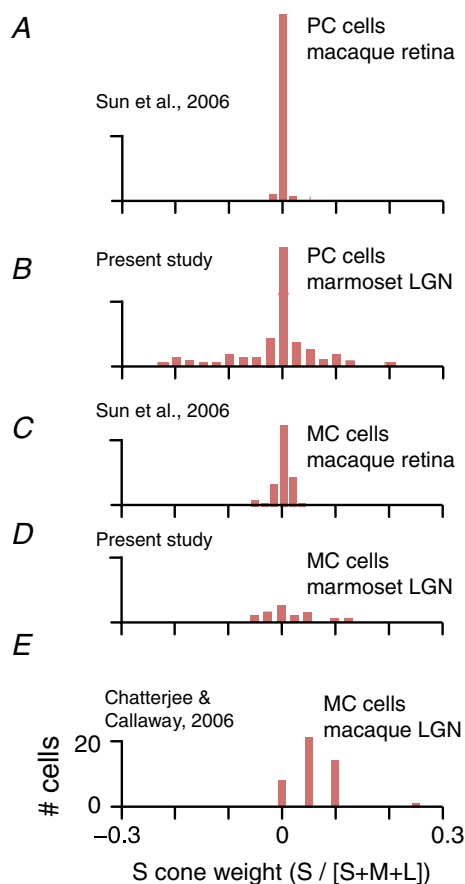

Figure 11. Comparison of S-cone inputs to parvocellular (PC) and magnocellular (MC) pathway cells estimated from three different studies

Positive S-cone weights indicate excitatory ('centre') S-cone inputs, negative weights indicate inhibitory ('surround') S-cone inputs. A, recordings from macaque PC-pathway retinal ganglion cells (Sun et al. 2006b; their Fig. 3). B, recordings from marmoset PC cells in the lateral geniculate nucleus (LGN). Data from the current study (Fig. 6). C, recordings from macaque MC-pathway retinal ganglion cells (Sun et al. 2006b; their Fig. 3). D, recordings from marmoset MC cells in the LGN. Data from the current study (Fig. 6). E, recordings from MC cells in macaque LGN (Chatterjee & Callaway, 2002; their Fig. 5).

cone fundamentals incorporating absorption by macular pigment (Stockman *et al.* 1993; Chatterjee & Callaway, 2002). When we tested an MC cell with the 'foveal' S-cone selective stimulus (Fig. 10*C–F*), the response was consistent with spurious ML-cone contrast. Furthermore, we found that in MC cells, the spatial and contrast transfer functions for S-cone selective gratings are simply scaled versions of their counterparts for ML-cone activating gratings (Fig. 9). These data suggest that the S-cone input to macaque MC cells was overestimated in Chatterjee & Callaway's study. Regardless of this specific issue, our results show that responses to nominally S-cone selective stimuli must be interpreted cautiously, and with reference to the contrast gain of the cell population being measured. Overall our results are more consistent with a bias against S-cone input to PC and MC cells; as suggested elsewhere (Sun *et al.* 2006*a*) such bias would protect high acuity spatial signals in MC and PC cells from degradation by out-of-focus wavelengths.

References

Baylor DA, Nunn BJ & Schnapf JL (1987). Spectral sensitivity of cones of the monkey *Macaca fascicularis*. *J Physiol* **390**, 145–160.

Blessing EM, Solomon SG, Hashemi-Nezhad M, Morris BJ & Martin PR (2004). Chromatic and spatial properties of parvocellular cells in the lateral geniculate nucleus of the marmoset (*Callithrix jacchus*). *J Physiol* **557**, 229–245.

Brainard DH (1996). Cone contrast and opponent modulation color spaces. In *Human Color Vision*, ed. Kaiser PK & Boynton GM, pp. 563–577. Optical Society of America, Washington, DC.

Calkins DJ, Tsukamoto Y & Sterling P (1998). Microcircuitry and mosaic of a blue-yellow ganglion cell in the primate retina. *J Neurosci* **18**, 3373–3385.

Chatterjee S & Callaway EM (2002). S cone contributions to the magnocellular visual pathway in macaque monkey. *Neuron* **35**, 1135–1146.

Chichilnisky EJ & Baylor DA (1999). Receptive-field microstructure of blue-yellow ganglion cells in primate retina. *Nat Neurosci* **2**, 889–893.

Chichilnisky EJ & Kalmar RS (2002). Functional asymmetries in ON and OFF ganglion cells of primate retina. *J Neurosci* **22**, 2737–2747.

Croner LJ & Kaplan E (1995). Receptive fields of P and M ganglion cells across the primate retina. *Vision Res* **35**, 7–24.

Dacey DM & Lee BB (1994). The 'blue-on' opponent pathway in primate retina originates from a distinct bistratified ganglion cell type. *Nature* **367**, 731–735.

Dacey DM, Lee BB, Stafford DK, Pokorny J & Smith VC (1996). Horizontal cells of the primate retina: cone specificity without spectral opponency. *Science* **271**, 656–659.

Dacey DM, Liao HW, Peterson BB, Robinson FR, Smith VC, Pokorny J, Yau KW & Gamlin PD (2005). Melanopsin-expressing ganglion cells in primate retina signal colour and irradiance and project to the LGN. *Nature* **433**, 749–754.

Dacey DM & Packer OS (2003). Colour coding in the primate retina: diverse cell types and cone-specific circuitry. *Curr Opin Neurobiol* **13**, 421–427.

Dacey DM & Petersen MR (1992). Dendritic field size and morphology of midget and parasol ganglion cells of the human retina. *Proc Natl Acad Sci U S A* **89**, 9666–9670.

Dacey DM, Peterson BB, Robinson FR & Gamlin PD (2003). Fireworks in the primate retina: in vitro photodynamics reveals diverse LGN-projecting ganglion cell types. *Neuron* **37**, 15–27.

DeMonasterio FM (1979). Asymmetry of ON- and OFF-pathways of blue sensitive-cones of the retina of macaques. *Brain Res* **166**, 39–48.

DeMonasterio FM & Gouras P (1975). Functional properties of ganglion cells of the rhesus monkey retina. *J Physiol* **251**, 167–195.

Derrington AM, Krauskopf J & Lennie P (1984). Chromatic mechanisms in lateral geniculate nucleus of macaque. *J Physiol* **357**, 241–265.

Einevoll GT & Plesser HE (2005). Response of the difference-of-Gaussians model to circular drifting-grating patches. *Vis Neurosci* **22**, 437–446.

Felius J & Swanson WH (2003). Effects of cone adaptation on variability in S-cone increment thresholds. *Invest Ophthalmol Vis Sci* **44**, 4140–4146.

Ferreras A, Polo V, Larrosa JM, Pablo LE, Pajarin AB, Pueyo V & Honrubia FM (2007). Can frequency-doubling technology and short-wavelength automated perimetries detect visual field defects before standard automated perimetry in patients with preperimetric glaucoma? *J Glaucoma* **16**, 372–383.

Field GD, Sher A, Gauthier JL, Greschner M, Shlens J, Litke AM & Chichilnisky EJ (2007). Spatial properties and functional organization of small bistratified ganglion cells in primate retina. *J Neurosci* **27**, 13261–13272.

Forte JD, Hashemi-Nezhad M, Dobbie WJ, Dreher B & Martin PR (2005). Spatial coding and response redundancy in parallel visual pathways of the marmoset *Callithrix jacchus*. *Vis Neurosci* **22**, 479–491.

Frishman LJ, Freeman AW, Troy JB, Schweitzer-Tong DE & Enroth-Cugell C (1987). Spatiotemporal frequency responses of cat retinal ganglion cells. *J Gen Physiol* **89**, 599–628.

Gegenfurtner KR & Kiper DC (2003). Color vision. *Annu Rev Neurosci* **26**, 181–206.

Ghosh KK & Grünert U (1999). Synaptic input to small bistratified (blue-On) ganglion cells in the retina of a New World monkey, the marmoset *Callithrix jacchus*. *J Comp Neurol* **413**, 417–428.

Ghosh KK, Martin PR & Grünert U (1997). Morphological analysis of the blue cone pathway in the retina of a New World monkey, the marmoset *Callithrix jacchus*. *J Comp Neurol* **379**, 211–225.

Goodchild AK, Ghosh KK & Martin PR (1996). Comparison of photoreceptor spatial density and ganglion cell morphology in the retina of human, macaque monkey, cat, and the marmoset *Callithrix jacchus*. *J Comp Neurol* **366**, 55–75.

Hashemi-Nezhad M, Blessing EM, Dreher B & Martin PR (2008). Segregation of short-wavelength sensitive ('blue') cone signals among neurons in the lateral geniculate nucleus and striate cortex of marmosets. *Vision Res* (in press; doi: 10.1016/j.visres.2008.02.017).

Irvin GE, Norton TT, Sesma MA & Casagrande VA (1986). W-like response properties of interlaminar zone cells in the lateral geniculate nucleus of a primate (*Galago crassicaudatus*). *Brain Res* **362**, 254–270.

Kilavik BE, Silveira LC & Kremers J (2003). Centre and surround responses of marmoset lateral geniculate neurones at different temporal frequencies. *J Physiol* **546**, 903–919.

Klug K, Herr S, Ngo IT, Sterling P & Schein S (2003). Macaque retina contains an S-cone OFF midget pathway. *J Neurosci* **23**, 9881–9887.

Kouyama N & Marshak DW (1992). Bipolar cells specific for blue cones in the macaque retina. *J Neurosci* **12**, 1233–1252.

Kremers J, Weiss S, Zrenner E & Maurer J (1997). Spectral responsivity of lateral geniculate cells in the dichromatic common marmoset (*Callithrix jacchus*). Rod and cone inputs to parvo- and magnocellular cells. In *Colour Vision Deficiencies XIII*, ed. Cavonius CR, pp. 87–97. Kluwer Academic Publishers, Dordrecht.

Lamb TD (1995). Photoreceptor spectral sensitivities: common shape in the long-wavelength region. *Vision Res* **35**, 3083–3091.

Lankheet MJM, Lennie P & Krauskopf J (1998). Temporal-chromatic interactions in LGN P-cells. *Vis Neurosci* **15**, 47–54.

Lee SCS & Grünert U (2007). Connections of diffuse bipolar cells in primate retina are biased against S-cones. *J Comp Neurol* **502**, 126–140.

Lee SC, Telkes I & Grünert U (2005). S-cones do not contribute to the OFF-midget pathway in the retina of the marmoset, *Callithrix jacchus*. *Eur J Neurosci* **22**, 437–447.

Malpeli JG & Schiller PH (1978). Lack of blue OFF-center cells in the visual system of the monkey. *Brain Res* **141**, 385–389.

Mariani AP (1984). The neuronal organization of the outer plexiform layer of the primate retina. *Int Rev Cytol* **86**, 285–320.

Marimont DH & Wandell B (1994). Matching color images: the effects of axial chromatic aberration. *J Opt Soc Am A* **11**, 3113–3122.

Martin PR, White AJR, Goodchild AK, Wilder HD & Sefton AE (1997). Evidence that blue-on cells are part of the third geniculocortical pathway in primates. *Eur J Neurosci* **9**, 1536–1541.

McLellan JS & Eskew RT (2000). ON and OFF S-cone pathways have different long-wave cone inputs. *Vision Res* **40**, 2449–2465.

McLellan JS, Marcos S, Prieto PM & Burns SA (2002). Imperfect optics may be the eye's defence against chromatic blur. *Nature* **417**, 174–176.

Puller C, Haverkamp S & Grünert U (2007). OFF midget bipolar cells in the retina of the marmoset, *Callithrix jacchus*, express AMPA receptors. *J Comp Neurol* **502**, 442–554.

Racheva K & Vassilev A (2008). Sensitivity to stimulus onset and offset in the S-cone pathway. *Vision Res* **48**, 1125–1136.

Reid RC & Shapley RM (2002). Space and time maps of cone photoreceptor signals in macaque lateral geniculate nucleus. *J Neurosci* **22**, 6158–6175.

Sceniak MP, Ringach DL, Hawken MJ & Shapley RM (1999). Contrast's effect on spatial summation by macaque V1 neurons. *Nat Neurosci* **2**, 733–739.

Sherman SM & Guillery RW (2006). *Exploring the Thalamus and its Role in Cortical Function*. MIT Press, Cambridge, MA, USA.

Silveira LCL, Lee BB, Yamada ES, Kremers J, Hunt DM, Martin PR & Gomes F (1999). Ganglion cells of a short wavelength sensitive cone pathway in New World monkeys: Morphology and physiology. *Vis Neurosci* **16**, 333–343.

Solomon SG, Lee BB, White AJ, Rüttiger L & Martin PR (2005). Chromatic organization of ganglion cell receptive fields in the peripheral retina. *J Neurosci* **25**, 4527–4539.

Solomon SG & Lennie P (2005). Chromatic gain controls in visual cortical neurons. *J Neurosci* **25**, 4779–4792.

Solomon SG, Peirce JW & Lennie P (2004). The impact of suppressive surrounds on chromatic properties of cortical neurons. *J Neurosci* **24**, 148–160.

Solomon SG, White AJR & Martin PR (1999). Temporal contrast sensitivity in the lateral geniculate nucleus of a New World monkey, the marmoset *Callithrix jacchus*. *J Physiol* **517**, 907–917.

Solomon SG, White AJR & Martin PR (2002). Extra-classical receptive field properties of parvocellular, magnocellular and koniocellular cells in the primate lateral geniculate nucleus. *J Neurosci* **22**, 338–349.

Stockman A, MacLeod DI & Johnson NE (1993). Spectral sensitivities of the human cones. *J Opt Soc Am A* **10**, 2491–2521.

Sun H, Smithson HE, Zaidi Q & Lee BB (2006*a*). Specificity of cone inputs to macaque retinal ganglion cells. *J Neurophysiol* **95**, 837–849.

Sun H, Smithson HE, Zaidi Q & Lee BB (2006*b*). Do magnocellular and parvocellular ganglion cells avoid short-wavelength cone input? *Vis Neurosci* **23**, 441–446.

Szmajda BA, Buzás P, FitzGibbon T & Martin PR (2006). Geniculocortical relay of blue-off signals in the primate visual system. *Proc Natl Acad Sci U S A* **103**, 19512–19517.

Szmajda BA, Martin PR & Grünert U (2008). Retinal ganglion cell inputs to the koniocellular pathway. *J Comp Neurol* **510**, 251–268.

Tailby C, Solomon SG & Lennie P (2008). Functional asymmetries in visual pathways carrying S-cone signals in macaque. *J Neurosci* **28**, 4078–4087.

Tovée MJ, Bowmaker JK & Mollon JD (1992). The relationship between cone pigments and behavioural sensitivity in a New World monkey (*Callithrix jacchus jacchus*). *Vision Res* **32**, 867–878.

Ts'o DY & Gilbert CD (1988). The organization of chromatic and spatial interactions in the primate striate cortex. *J Neurosci* **8**, 1712–1727.

Valberg A, Lee BB & Tigwell DA (1986). Neurones with strong inhibitory S-cone inputs in the macaque lateral geniculate nucleus. *Vision Res* **26**, 1061–1064.

Webb BS, Tinsley CJ, Vincent CJ & Derrington AM (2005). Spatial distribution of suppressive signals outside the classical receptive field in lateral geniculate nucleus. *J Neurophysiol* **94**, 1789–1797.

White AJR, Goodchild AK, Wilder HD, Sefton AE & Martin PR (1998). Segregation of receptive field properties in the lateral geniculate nucleus of a New-World monkey, the marmoset *Callithrix jacchus*. *J Neurophysiol* **80**, 2063–2076.

White AJR, Solomon SG & Martin PR (2001). Spatial properties of koniocellular cells in the lateral geniculate nucleus of the marmoset *Callithrix jacchus*. *J Physiol* **533**, 519–535.

Wiesel TN & Hubel D (1966). Spatial and chromatic interactions in the lateral geniculate body of the rhesus monkey. *J Neurophysiol* **29**, 1115–1156.

Young T (1802). The Bakerian Lecture. On the theory of light and colours. *Philos Trans R Soc Lond* 12–48.

Zlatkova MB, Vassilev A & Anderson RS (2008). Resolution acuity for equiluminant gratings of S-cone positive or negative contrast in human vision. *J Vis* **8**, 9.1–10.

Zrenner E & Gouras P (1981). Characteristics of the blue sensitive cone mechanism in primate retinal ganglion cells. *Vision Res* **21**, 1605–1609.

Zrenner E & Gouras P (1983). Cone opponency in tonic ganglion cells and its variation with eccentricity in rhesus monkey retina. In *Colour Vision: Physiology and Psychophysics*, ed. Mollon JD & Sharpe LT, pp. 211–223. Academic Press, London.

Acknowledgements

Authors current address

Brett Szmajda, Department of Ophthalmology, Northwestern University, Chicago, USA.

Peter Buzás, Institute of Physiology, University of Pécs, Hungary.